UNDERSTANDING THE EFFECTS OF HUMAN EPIGLOTTIS STRUCTURE ON AIRFLOW DYNAMICS USING CFD

By

Lingmeng Li

Thesis for Master of Research in
Biomedical Engineering

Department of Engineering
Macquarie University

Submission date: 17th May 2018

Supervisor: Dr. Shaokoon Cheng

Declaration

I, Lingmeng Li, declare that this thesis is a part of the requirement for the award of Master of Research, and this degree is also a research training pathway program leads to the Ph.D. at Macquarie University. This thesis is entirely my outcomes except otherwise referenced or acknowledged. There is no content which has been previously published by any other author or academic institution.

Student's name: Lingmeng Li

Student's signature:

Date: 05/07/2018

Abstract

This thesis is written for the Master of Research Program at Macquarie University, the objective of this project is to understand the real-time respiratory flow in a human upper airway. Airflow in the human upper airway is of paramount importance given its role in the delivery of particles to the human lungs. The structure of the human upper airway plays a critical role in understanding airflow dynamics along the respiratory tracts. Currently, even basic information on how differences in the upper airway geometry effect regional airflow dynamics along the human upper airway is limited. This project aims to study how the epiglottis structure affects the respiratory flow by performing computational fluid dynamics analysis on 3D human upper airway models reconstructed from MRI, and the changes in airflow pattern as a function of epiglottis position and structure will be investigated. This thesis concludes with a discussion of how the position and structure of the epiglottis contributed to the airflow behaviours in the human upper airway, decrease in airway diameter at the level of epiglottis increase velocity significantly which also appears to influence the spatial pressure distribution extensively such that it covers a large region of the upper airway. Emphasis was also given to address the simulation conditions that should be used when performing transient flow simulations in the human upper airway.These results imply a potential change in particles fluidization dynamics in the upper airway given a small change in anatomical structure although further studies need to be performed to understand this is detail.

Contents

List of Figures

List of Tables

Abbreviations

OSA: *Obstructive Sleep Apnea*

MRI: *Magnetic Resonance Image*

CT: *Computed Tomography*

CFD: *Computational Fluid Dynamics*

COPD: *Chronic Obstructive Pulmonary Disease*

ATM: *Standard atmospheric pressure*

PIV: *Particle Image Velocimetry*

TKE: *Turbulent Kinetic Energy*

DNS: *Direct Numerical Simulation*

LES: *Large Eddy Simulation*

RANS: *Reynolds Averaged Navier-Stokes*

3D: *3-dimensions*

Re*: Reynolds Number*

Nomenclature

f: Breathing frequency

Tb: Breathing period

V: Total inspiration volume

U: Mean velocity of the flow

D: Hydraulic diameter

p: Pressure

v: Dynamic viscosity

ρ: Density

Acknowledgment

I would like to acknowledge Dr. Shaokoon Cheng, Mr. Taye Mekonnen, Mr. Sajjad Mahmoudi and Mr. Joel Raco for their encouragement.

Firstly, Dr. Shaokoon Cheng was my supervisor for the entire project, and he has provided professional training and personal support. I have learned much knowledge and research attitude over the past eight months.

Many thanks to my team members, Mr. Taye Mekonnen, Mr. Sajjad Mahmoudi and Mr. Joel Raco, for their help and advice on my research.

Finally, I would like to thank the Higher Degree Research office of Macquarie University for providing the funding and technical support for this project.

CHAPTER 1

INTRODUCTION

1.1 Significance

Respiration is one of the essential biological processes in the human body. The primary function of respiration is to supply oxygen from ambient air and remove carbon dioxide from the human body. During respiration, harmful particles may be inhaled into human bodies, and the particles may lead to a wide range of respiratory diseases, such as common cold, nasal cancer, and asthma exacerbations. In the United States alone, more than one billion people suffer from common cold each year, and there are approximately fifteen million asthmatic patients exist. In addition, according to the records, around 2% to 4%, and more than 10% of the population has been estimated to suffer from OSA and sinusitis respectively (Kaliner et al., 1997, Mannino et al., 1998, Mygind and Dahl, 1998, Young et al., 1993). There are more than 64 million people who are currently suffering from COPD worldwide (N. L. Phuong et al., 2015). Despite the fact that the afore-mentioned problems are related to the disruption of normal airflow in the human respiratory tracts, necessary information of how airflow dynamics is influenced by the complex structure of the human upper airway and nasal cavity remains unclear. More specifically, there is a complete lack of understanding of how airflow pattern is affected at critical regions of the human upper airway, such as the epiglottal region, and how the structure of the epiglottis may affect the airflow pattern in the lower airway downstream. Therefore, it is crucial to advance our understanding in this area by providing new insights into how airflow changes as a function of the position and structure of epiglottis in the human upper.

1.2 Human Upper Airway Anatomy and Mechanical Properties

The human upper airway has a very complex structure and varies widely among individuals. A comprehensive understanding of the anatomy and properties of the human upper airway is essential to study the airflow pattern in the human upper airway.

The structure of the human upper airway plays a vital role in particle deposition as airflow, and the particles are guided by its geometry. Many processes take place as air enters the airway, which are

essential respiratory functions that include basic air transportation, gas exchange, air warming, air filtration and humidification. (G. Mylavarupu, 2013; C. Li et al., 2017).

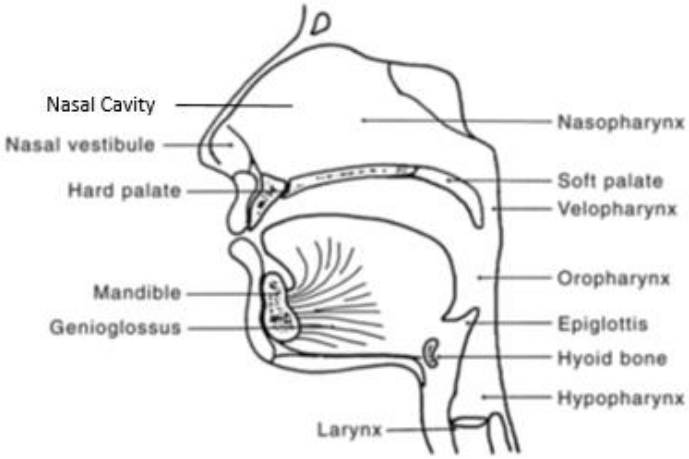

Figure 1.1 Anatomical landmarks of the human upper airway (R. Pearce et al., 1999).

Figure 1.1 shows a typical human upper airway and the fundamental structures that belong or form the part of the passageway. They are the nasal cavity, the tongue, the epiglottis and the lower airway lumen. Conventionally, the upper airway has also been sectioned and described as four distinct regions, which are:

1. Nasopharynx (NP): from nostrils to posterior end of the hard plate.
2. Retropalatal pharynx (RP): behind the soft plate.
3. Retroglossal pharynx (RG): behind the tongue.
4. Hypopharynx (HP): from the tongue to the larynx (G. Mylavarapu et al., 2013).

The nasal cavity has two separate passageways with irregular shapes connected by the nasal septum, which is located in the middle of the two passageways. The nostrils which are at the anterior section of the nasal cavity is connected to the main pharynx by the choanae. The vestibule of the nasal cavity is only 30-40 mm^2 known as the narrowest region in the human upper airway (Proctor and Andersen, 1982). The entire pharyngeal airway is covered by soft tissues, cartilages, bones and muscles (Fouke et al., 1986). The retropalatal airway is also known as the velum connects the choanae to the soft palate. The retroglossal airway is the section of the upper airway that is located caudal to the velum which extends to the epiglottis. The epiglottis is made up of cartilages and epiglottis acts as a valve that enables human's breathing and swallowing. The diameter of the epiglottis has the smallest value in the upper airway as shown in **Figure 1.2**.

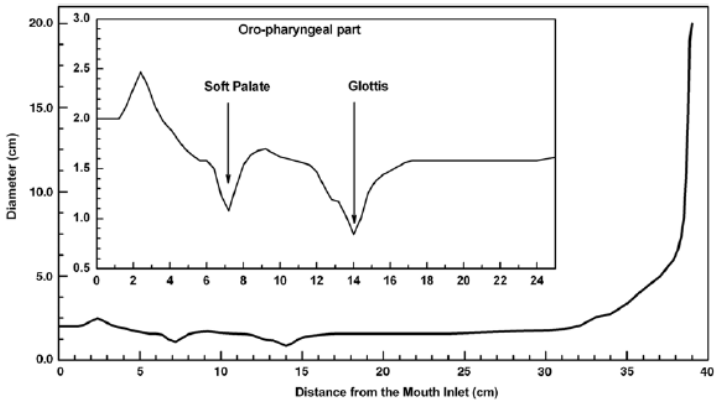

Figure 1.2: Variation of upper airway diameters as a function of distance in the anterior-posterior direction from the mouth inlet (J. Huang et al., 2013).

1.3 Functions of Tissues within Human Upper Airway.

The human upper airway is covered with different types of the mucosa, which have critical functions during normal respiration. Firstly, as the first physical barrier against bacteria and viruses in the air, the mucosa traps unwanted particles before they enter the lungs. Secondly, the epithelial mucosa provides purification, warming and humidification liked to an air processor. The submucosal vascular system is widely found in the nasal cavity, and the feather of the submucosal vascular network determines the calibre of the nasal passageway significantly. Another tissue type that is important to maintain the effective function of the human upper airway is the cartilage. In fact, the cartilage ring is one of the most important tissues that supports and protects the pharyngeal wall while other tissues such as vascular network and muscles help to determine the geometry and structure of the upper airway (T. Lai, 2011).

1.4 Background

1.4.1 Dynamic Motion of the Human Upper Airway.

A full respiratory cycle consists of the inspiratory phase and the expiratory phase. During regular inspiration, airway muscles enlarge the airway volume and the air into the lung is a result of the negative alveolar pressure caused by the simultaneous action of diaphragm contraction and rib cage expansion (J. Huang et al., 2013). The average breathing rate in a healthy adult is between 7 to14 L/min（G. Mylavarapu et al., 2013), and there are several vital parameters have been commonly used to describe characteristics of airflow profile, such as the peak inspiration flow rate, respiration frequency (*f*), breathing period (T_b), and total inspiration volume (V). **Figure 1.3** and **Figure 1.4**

illustrate a sine wave which is commonly used to represent an ideal respiratory cycle profile and an actual respiratory cycle profile respectively (G. Mylavarapu et al., 2013).

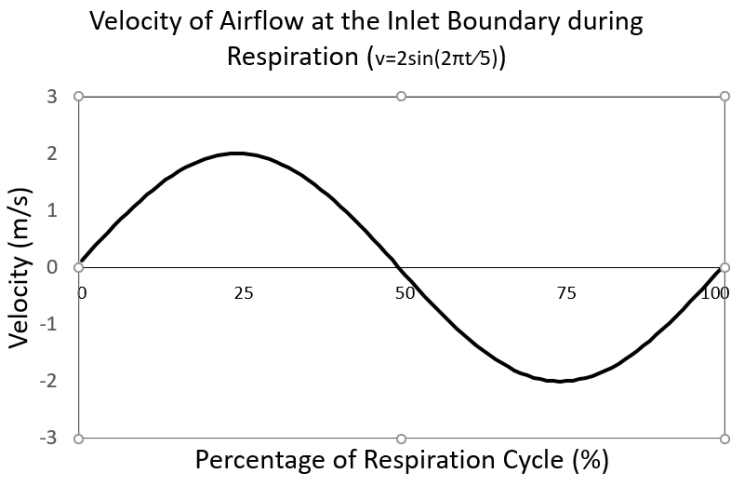

Figure 1.3: Respiratory flow.

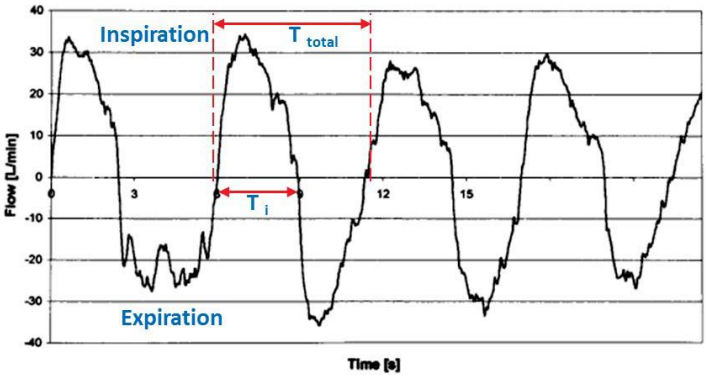

Figure 1.4: A typical respiratory flow profile at nostrils of a human breathing pattern at rest (G. Mylavarapu et al., 2013).

1.4.2 Treatment Using Inhaler Device

The respiratory inhaler is a well-established method to deliver drug particles to the pulmonary system. About 4000 years ago, inhalers were applied to treat respiratory diseases in India (J. Grossman 1994). In the 19th and 20th century, inhaler technology made considerable progress with the industrial revolution. Inhalers have since become the most widely used medical device to treat respiratory diseases, such as asthma, bronchitis, and pneumonia, due to their advantages of inexpensive, easy to use, non-invasive and effective in delivering drugs.

Nevertheless, there are some inherent and existing drawbacks of inhalers that require improvements in innovation given the fact that current devices are not personalized. Indeed, current practices entail that the same inhaler may be prescribed to patients regardless of their gender, age and disease severities. Hence, this implicates several of problems that may aggravate the state of illness of the patients who are suffering from respiratory diseases. For example, differences in the upper airway structure as a function of age and disease severity is likely to affect the airflow rate, and airflow rate will inevitably change drug dosage, drug loss and deposition in the human airway. Based on a recent review, some suggestions for inhalers improvements are summarized as follows (A. Briggs et al., 2012):

1. Reduce the drug deposition in the upper airway, optimize lung deposition.
2. Easy to clean and can be reused.
3. Universal to all particle sizes and shapes.

Hence, inhaler devices and the drug delivery process can be improved in many ways, and it is essential to have a thorough understanding of factors that may affect the airflow pattern in the human upper airway.

1.4.3 Application of CFD to Biological Systems Modelling

CFD could provide details of fluid velocities, pressures, particle concentrations and temperatures by using numerical methods and analyse to solve and analyse the flow-governing equations (Navier-Stokes equations) (Cheng et al., 2014, Mihaescu et al., 2008).

CFD is not an inexpensive tool. Given the fact that it is difficult to obtain accurate flow field measurements in a biological system even with the use of invasive instruments, and fills the knowledge gap as a non-invasive and precise approach to study flow phenomena when certain boundary conditions are prescribed. (Y. Fan et al., 2011). To date, much biomedical research has been undertaken using CFD, and the work includes and is not limited to aerosol drug delivery, blood pumps, artificial heart valves, blood oxygenators' filtration devices, needles and catheters, tubing and diagnostic equipment (T. Lai, 2011).

1.5 Objectives and Aims

In this research project, the airflow in a 3D model of the human upper airway will be investigated using CFD. The methodologies that have been taken and described as follows:

1. A 3D human upper airway model reconstruction.
2. Modify the position and structure of the epiglottis (changing the distance between epiglottis tip and the back of the pharyngeal wall) to achieve another five models.
3. Investigate the airflow dynamics in six human upper airway models using CFD, and monitor how the positon and structure of the epiglottis affect airflow behaviours.
4. Provide an accurate simulation of local velocity and pressure distribution based on a realistic respiratory flow profile.
5. Compare changes in local velocity, pressure and other airflow behaviours of the human upper airway and to determine the influence of airflow changes as a function of epiglottis positions and structures.
6. The summarized limitation will be given and make recommendations for our future research.

The hypothesis here is that airflow behaviour is affected by the position and structure of epiglottis related to the back pharyngeal wall, and upper airway diameter at the epiglottis level has a significant effect on flow downstream in the lower respiratory tracts.

1.6 Perceived Contributions of the Research

This research project is expected to provide new information on how airflow behaviours may be affected by the position and structure of the epiglottis. Based on existing MRI studies, the structure of the epiglottis and the lumen size at the level of the human upper airway vary widely among individuals even when they have the same BMI and basic upper airway dimensions, such as the upper airway length. Given that the upper airway diameter at the level of the epiglottis is narrow and is the critical entry point before air transcends downstream to the tracheal and lower respiratory tracts, it is hence imperative to study how this critical section of the airway affects the flow dynamics. This will pave the way to improve the understanding of drug deposition and dosage as they travel pass the epiglottis.

1.7 Thesis Structure

This thesis is composed of five chapters. The content of each chapter is summarized as follows:

- **Chapter 1. Introduction**. This chapter will provide the background and information on the significance of this research. A detailed description of upper airway anatomy and tissues will be delivered. A brief introduction of CFD applications together with other basic information of this thesis, such as the project outline, perceived contribution of the project and thesis structure will be presented.
- **Chapter 2. Literature review.** A literature review of existing studies on the human upper airway will be involved in this chapter. The literature review covers some of the research methods were applied in previous studies.
- **Chapter 3. Methodology.** This chapter will provide detailed information about the methodologies were used in this project. Details of 3D models reconstruction, and the result of mesh independence tests are included in this chapter.
- **Chapter 4. Result.** This chapter will explain the numerical results of fluid flow in human upper airway simulated using CFD, and the results include velocity distribution, pressure distribution, and cross-sectional analysis.
- **Chapter 5. Conclusion.** This section will summarize and discuss the findings and discoveries made in this research project. Discussion, limitations and proposed goals for further research will be established.

CHAPTER 2

LITERATURE REVIEW

2.1 Introduction

The following chapter will review the detailed research methods and results in previous studies of upper airway flow dynamics research. These studies have been performed to understand how turbulence, boundary conditions, upper airway shapes and other factors affect the airflow behaviours in the human upper airway.

2.2 Review of Previous Studies

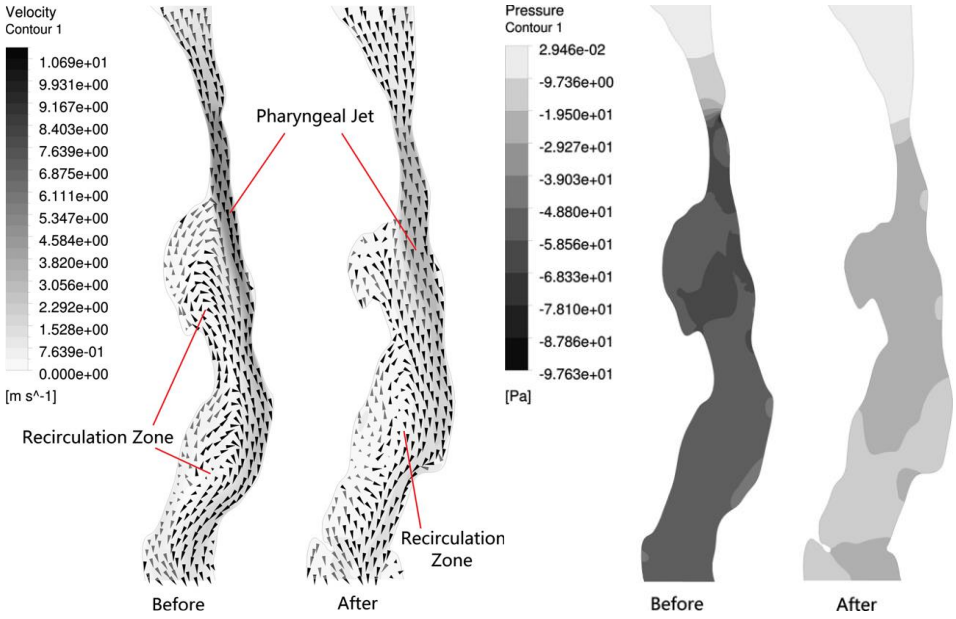

Figure 2.1: Velocity vectors and the 2D pressure contours in the middle vertical plane of the airway for Responder. Before: before MAS treatment. After: after MAS treatment (M. Zhao et al., 2013).

In 2013, M. Zhao et al. demonstrated that Mandibular Advancement Splints (MAS) is an effective treatment method for OSA by enlarging the airway space to prevent upper airway collapse (M. Zhao et al., 2013). The objective of the study was to investigate the potential of using CFD to predict the treatment response of OSA patients to MAS treatment. In this study, anatomically accurate upper

airway models were reconstructed from MRI data. Results from this study show that CFD can be indeed used as a useful tool to predict the treatment outcome of OSA patients using MAS (M. Zhao et al., 2013).

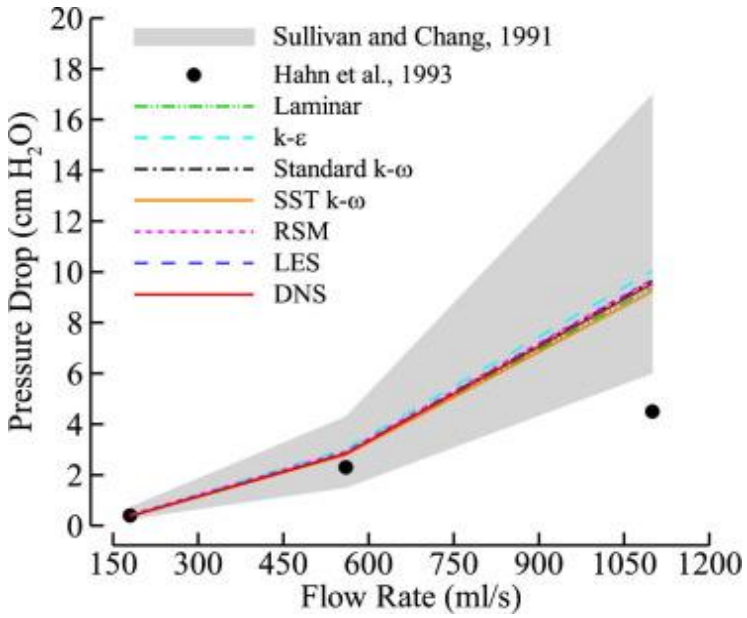

Figure 2.2: Comparison of pressure drop between current numerical simulations and previous experimental measurements at various flow rates. The grey shaded area represents the range of measured pressure drop by (Sullivan and Chang, 1991) in human subjects. The black dots indicate the experimental measurements in nasal cavity model (Hahn et al., 1993) (C. Li et al., 2017).

A recent study by C. Li et al. in 2017, is notable as this study was based on a 3-dimensional model of the human of the nasal cavity (C. Li et al., 2017). This study applied the basic laminar model, four RANS models, LES model and direct numerical simulation (DNS), The results showed that the laminar model gave a good agreement with the experimental results when the inlet velocity is 180 ml/s (Under rest breathing situation). RANS model performed better when the inlet flow rate is higher than 180 ml/s. LES and DNS have the most accurate result among all numerical models under all selected flow rates due to their calculating theory (C. Li et al., 2017). This study provides insights into the choice of a suitable CFD numerical scheme for airflow modelling.

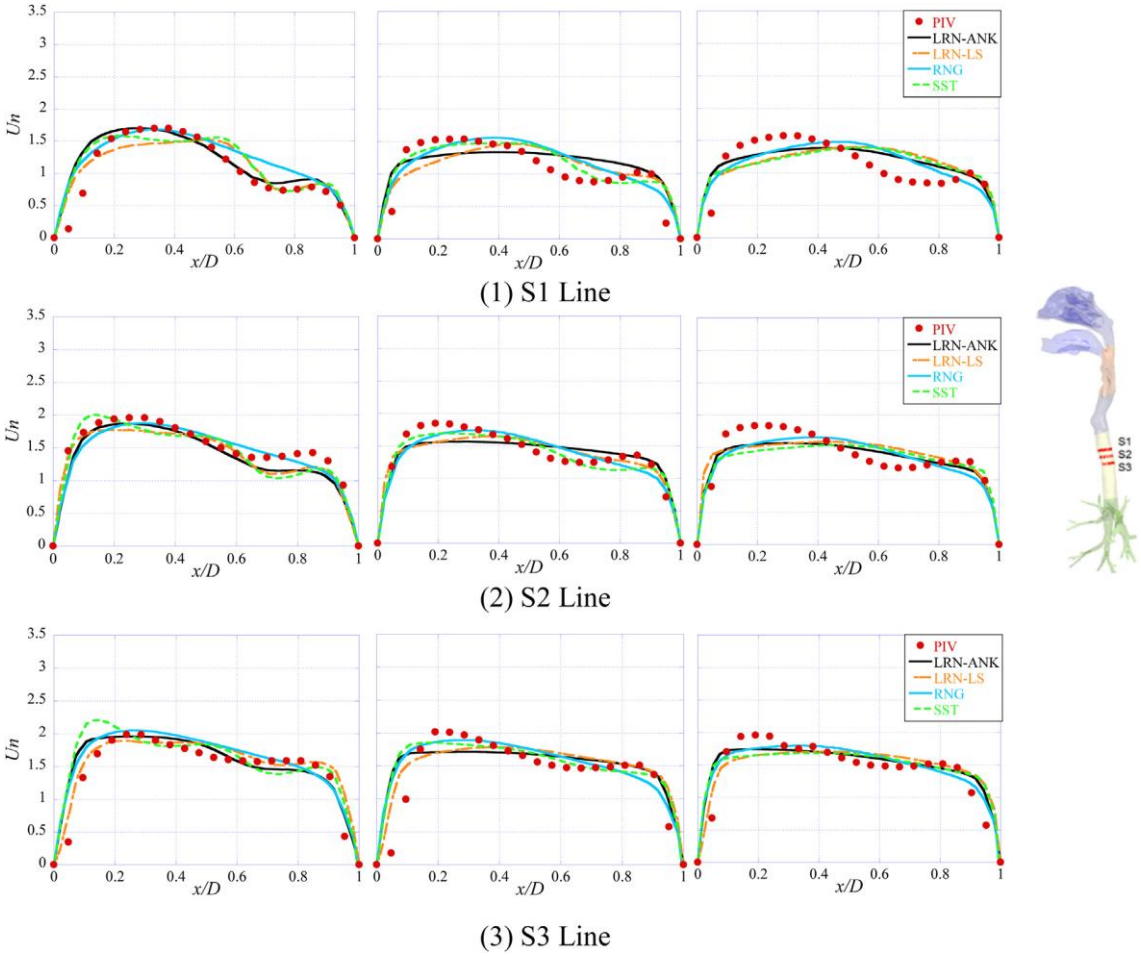

Figure 2.3: Profiles of normalized scalar velocity under Nasal Breathing Condition (Left: 7.5 L/min, Centre: 15 L/min, Right: 30 L/min) (N. L. Phuong et al., 2015).

In 2015, N. L. Phuong et al. used four RANS turbulence models (two low-Reynolds number type k-ε turbulence models, RNG k-ε model and SST k-ω model） to predict the airflow characteristics in a reconstructed human upper airway (N. L. Phuong et al., 2015). In this study, the LR-ANK k-ε turbulence model has the best agreement with the experimental data.

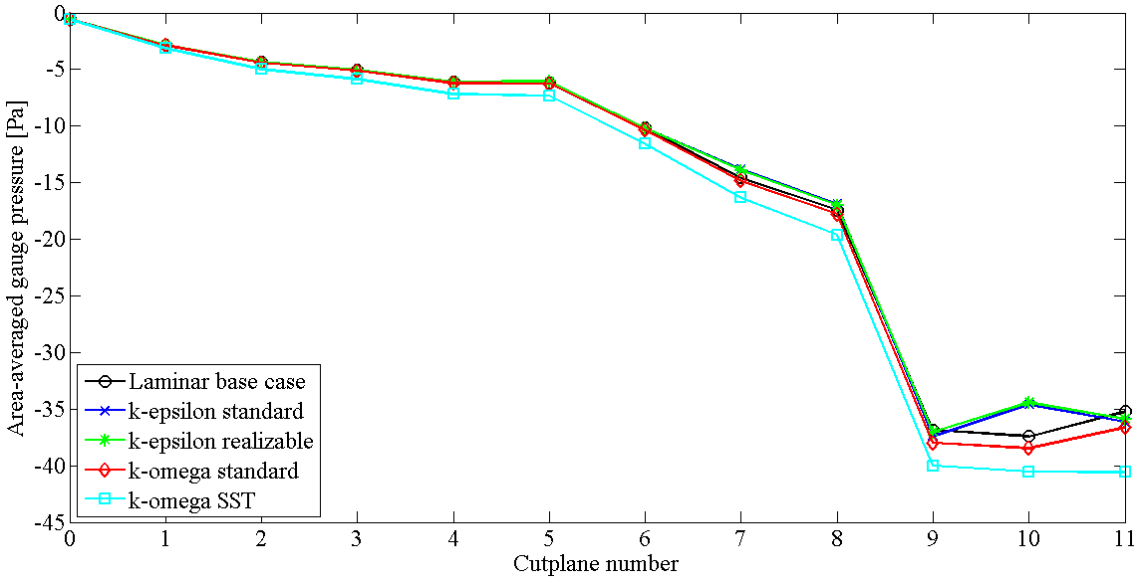

Figure 2.4: Comparison of area-averaged pressure for the laminar base-case and four different turbulence models (E. Aasgrav et al., 2017).

E. Aasgrav et al. presented a paper during the 12th International Conference on CFD in Oil & Gas, Metallurgical and Process Industries in 2017 (E. Aasgrav et al., 2017). In this paper, four different standard RANS turbulence models and a laminar flow model were used to investigate airflow characteristics during inspiration. The authors compared five different models using a constant flow rate of 250 ml/s. The author concluded that difference in the turbulence schemes does not influence the results of CFD simulation at least for the chosen patient's upper airway. A limitation of this study is that only a single flow rate has been used and more flow rates need to be investigated in the future (E. Aasgrav et al., 2017).

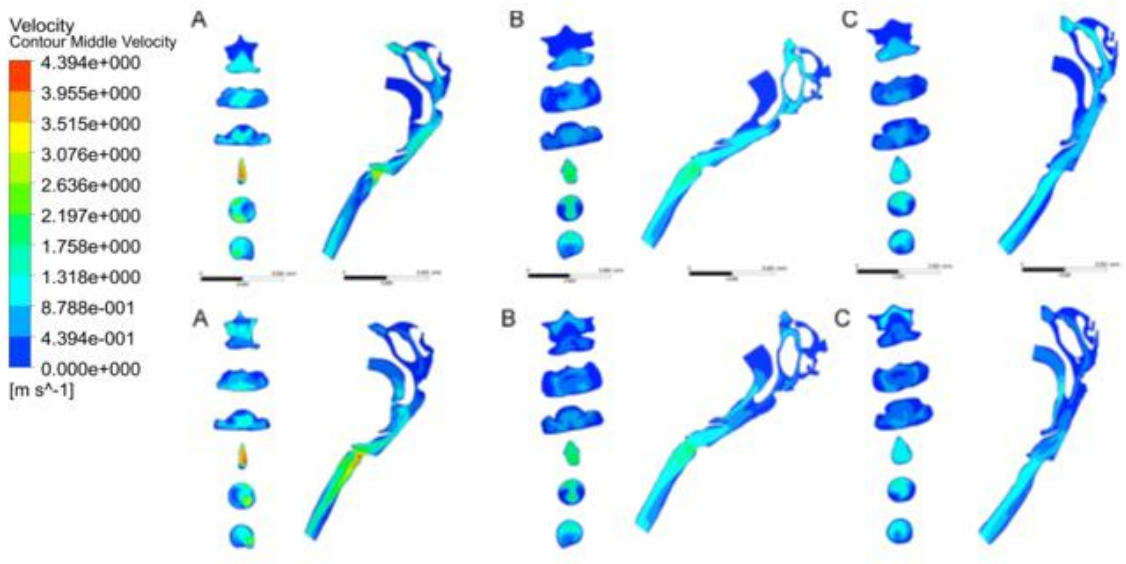

Figure 2.5: Velocity contour of cross-sectional areas in the hypopharynx, epiglottis, glottis, and trachea in different positions. (I) Closed-mouth situation and (II) open-mouth situation in the (A) neutral position, (B) extension position, and(C) sniffing position (W. Wei et al., 2017).

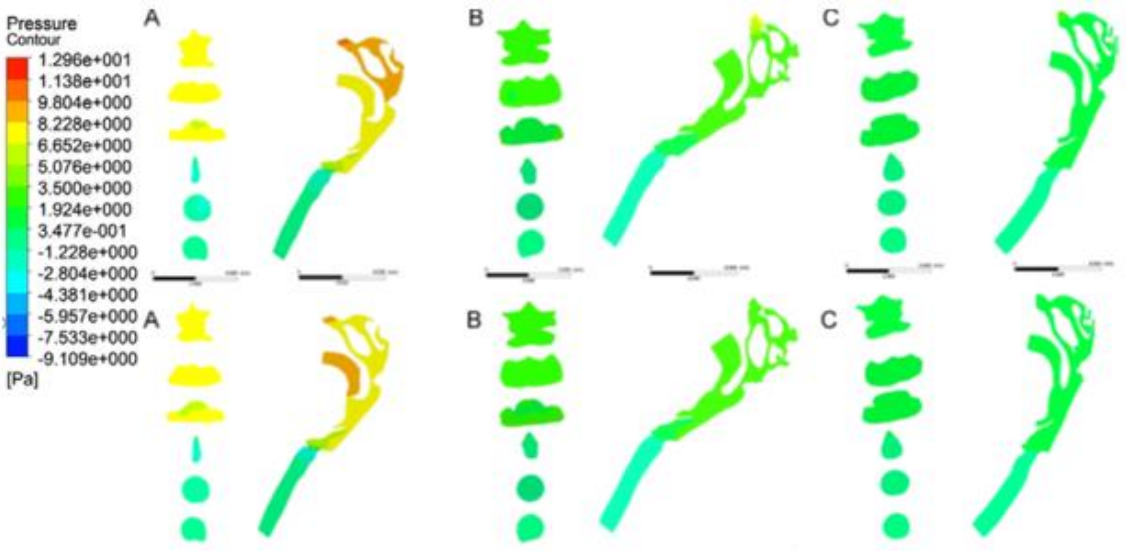

Figure 2.6: Pressure contour of cross-sectional areas in the hypopharynx, epiglottis, glottis, and trachea in different positions. (I) Closed-mouth and (II) open-mouth ventilation in the (A) neutral, (B) extension, and (C) sniffing positions (W. Wei et al., 2017).

In the paper published by W. Wei et al. in 2017, the effects of different head and neck positions on airflow patterns were simulated using CFD (W. Wei et al., 2017). The authors concluded that airway could be enlarged from head and neck positioning which allows for higher airflow. According to the study, changes in the geometry of the airway may influence the airflow profiles at different levels of the airway significantly (W. Wei et al., 2017).

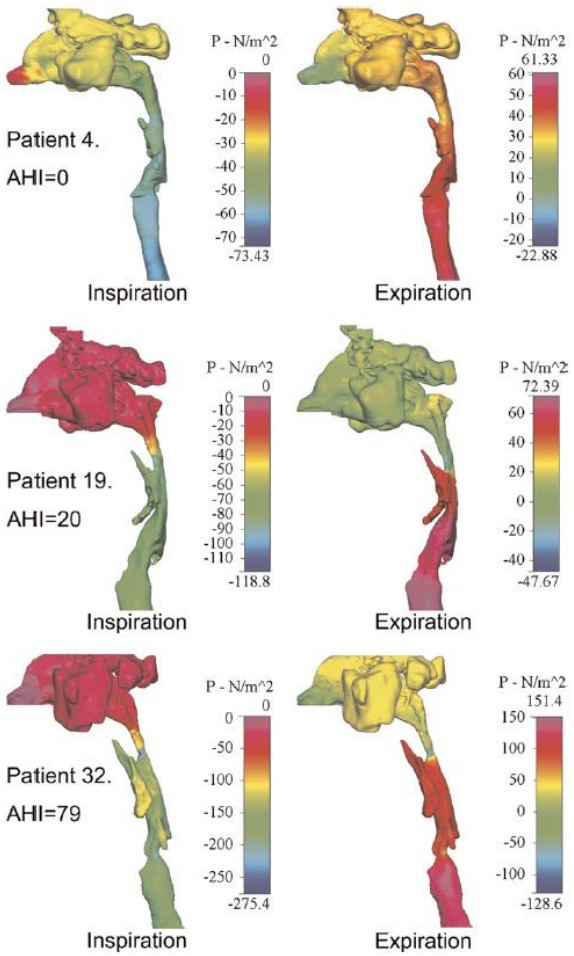

Figure 2.7: Visualization of the anatomic shape and pressure gradient of 3 patients from different AHI groups by CFD simulations. The pressure gradient across the whole airway is smoother in patient 4, and her nasal passage carries most of the pressure drop. The magnitude of the pressure drop in Amin is much more than through the nasal passage in patients 19 and 32. This phenomenon is even more obvious in patient 32 than in patient 19 (C. Yu et al., 2012).

In 2012, C. Yu et al. performed studies on the inspiratory phase using 3D models of the human upper airway with severe OSA (C. Yu et al., 2012). The study demonstrated a strong relationship between the pressure drop across the upper airway CFD models and the patient's apnea-hypopnea index (C. Yu et al., 2012). Also, the narrow airways as commonly observed in OSA patients increase the turbulence kinetic energy of airflow significantly (C. Yu et al., 2012). This work is coherent with the research of M. Mihaescu et al. in 2008, who showed that flow velocity and wall shear stress are high in regions of the upper airway with small a cross-sectional area. According to that study, understanding wall shear stress and their effects on the human airway wall may be important to improve current understanding of the pathophysiology of OSA (Mihaescu et al., 2008).

2.3 Imaging Datasets and 3D Slicer

The development of radiological techniques provides a practical approach to obtain accurate datasets of human anatomical structures. 3D models are usually reconstructed using images obtained from computed tomography (CT) scan or Magnetic Resonance Imaging (MRI) (C. C. Yu et al., 2012; M. Rahiminejad et al., 2016; Allen et al., 2004; Sung et al., 2007).

MRI data post-processing software includes 3-Matic, MIMICS and 3D Slicer (J. Tan et al. 2013). While these programs have their strengths and weaknesses, 3D Slicer has been chosen for this project as it is a free and open source software. Furthermore, 3D Slicer offers a wide range of features for visualization, exploration and quantitative analysis of imaging data (A. Fedorov et al., 2012).

2.4 Application of CFD in respiratory airways

In recent years, Computational Fluid Dynamics (CFD) simulations in different parts of the human respiratory tract have been studied by several researchers (Kleinstreuer and Zhang, 2010; Park and Wexler, 2008; Wang et al., 2009). Besides using the CFD models to understand basic flow field in a patient-specific airway, other aspects of the flow field, such as the laminar-to-turbulence transition, skewed velocity profiles in the lower respiratory tracts, complex recirculation and secondary flow have also been investigated. All these flow behaviour are likely to have an impact on particle transport and deposition (J. Huang et al., 2013), although the field in simulating laden particle flow remains primitive due to the lack of experimental data to validate the models and the inherent superfluous assumptions embedded in the computational codes. CFD applies numerical methods and algorithms to analyse problems involving fluid flow, and the computationally expensive procedure is often assisted by using high-end computers (C. C Yu et al., 2012).

The core of CFD calculation is the computational grid, which is used to divide the solution domain into c in which the problem variables are computed and stored (M. K. Gokcan et al., 2016). In recent studies, mesh generation in the 3D models has been commonly created using ANSYS ICEM CFD (C. C. Yu et al., 2012; V. Goodarzi-Ardakani et al., 2016), mesh generator Gambit 2.2 (Fluent Inc., Lebanon, New Hampshire) (Mihaescu et al.) and ANSYS Meshing (ANASYS, 2017).

2.5 Turbulence

Although different turbulence models are currently available in commercial CFD packages (G. Mylavarapu et al., 2009) (e.g. standard k-ω, transient flow k-ω, SST k-ω, low-Reynolds k-ε and k-ε with enhances wall treatment), it is important to be reminded that accuracy of a turbulence model is dependent on the type of application, and experimental data would be ideal to support the results generated from the simulations (M. Rahiminejad et al. 2016). While the standard k-ω turbulence model has been demonstrated to be a better predictor of flow with wall static pressure (G. Mylavarapu et al., 2009) and has good agreement with experimental results, the standard k-ε model proposed by Launder and Spalding (B. E. Launder et al., 1972) is the most widely used model in conventional engineering applications. The RNG model is excellent for simulating rapidly strained and swirled flows and has been demonstrated to be more accurate and reliable for a broader type of flows (Y. Wang et al., 2017) compared to other models. The realizable model has been proven to have superior performance for flows with strong streamline curvature, vortices and rotation. Compared to standard k-ε model, the realizable model has a modified transport equation for the dissipation rate and contains an alternative formulation for the turbulent viscosity (Y. Wang et al., 2017).

2.6 Airflow Rate

Most of the existing studies on the CFD modelling of human respiratory flow have used constant inlet flow rate, which is unrealistic as the transient and time-dependent effects of realistic respiratory flow are ignored. Air is defined as incompressible in existing studies (V. Goodarzi-Ardakani et al., 2016) and the constant flow rates that have been used to simulate inhalation in the literature vary widely among published studies. For example, while Y. Fan et al. used a constant volume flow rate of 0.3 L/s, M. Mihaescu et al.'s used four different flow rates (3L/min, 5 L/min, 10 L/min, and 15 L/min) that are distinctively higher. It is important to note that the airflow rate for adults can range between 5-12L/min for light breathing and 12-40 L/min during exertion and heavy exercise (V. Goodarzi-Ardakani et al., 2016). To get accurate results, ideally, peak airflow rates (5-40 L/min) and pulsatile flow ought to be considered (Jeong S. J. et al. 2007). The numerical results for fluid flow and particle deposition have been reported by (Zhang et al., 2010), but these studies have used a constant flow rate, and hence, the particles were injected at a constant rate. Therefore, while the study provided some insights into particle transport in the airway, the models are unlikely to have successfully replicated the actual particle transport process in an airway. Indeed, it is important to study how the transient effects on particle deposition based on a realistic pulsatile flow.

2.7 Boundary Conditions

In the majority of the existing studies on the computational modelling of airway flow, the fluid inhaled was considered to be normal air. The density and dynamic viscosity were usually defined as 1.1614kg/m^3 and 1.846*10^{-5}kg/m*s respectively (e.g., C. C. Yu et al., 2012). Also, the inlet boundary and outlet boundary were defined as 1 ATM (standard atmospheric pressure), the walls of the domain were assumed rigid, and no-slip boundary conditions have been prescribed (V. Goodarzi-Ardakani et al., 2016; C. C Yu et al., 2012). Turbulence intensity of 5% and turbulent viscosity ratio of 10 (E. Aasgrav et al., 2017; G. Mylavarapu et al., 2009) were also commonly prescribed in the models. The parameters mentioned above will be utilized in this project, and other important physiological flow conditions also will be listed in section 3.5 and 3.6.

2.8 Conclusion and Research Directions

While there are a handful of studies on the computational modeling of airway flow, knowledge on how some distinctive anatomical structures of the airway affect the flow is limited and more studies in this area are needed, this knowledge is a significant knowledge gap to fill since it is essential to consider the variation in some of these airway structures as they are likely to affect the airflow and particle transport and deposition. In this project, information such as how cross-sectional velocity distribution, pressure distribution and streamlines are affected by the epiglottis in human upper airway will be presented.

CHAPTER 3

METHODOLOGY

3.1 Geometry Creation

In order to have an accurate upper airway model, high-resolution axial MRI datasets (Pixel resolution 0.25mm * 0.25mm* 0.25mm) of the mechanical upper airway model were acquired from the open source program 3D slicer. CFD simulations were conducted to investigate the airflow profiles at various sections of the model. **Figure 3.1** shows the full geometry of the reconstructed upper airway.

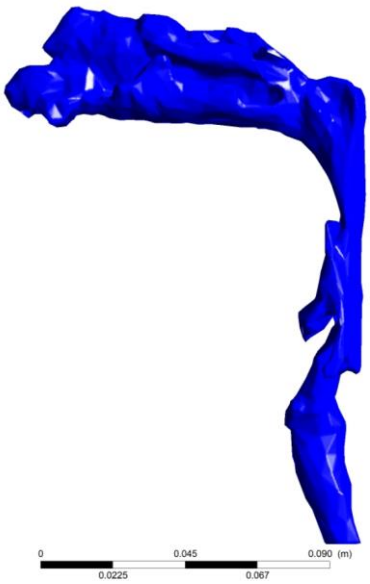

Figure 3.1: Screen capture of model reconstructed using 3D Slicer.

3.2 Numerical Methodologies

3.2.1 Flow regimes

Turbulent flow is ubiquitous in many biological flows and engineering applications. Based on existing turbulence models, majority of them enables a mean flow to be obtained, and there are inherent limitations in obtaining a description of the detailed time-resolved flow field due to the turbulent fluctuations. Hence there is a need to develop turbulence models that are both accurate and computationally efficient for broad applicability in airway studies (Y. Wang et al., 2017).

Laminar, transitional and turbulent are three different flow regimes that are represented by different sets of Reynolds number which is a dimensionless number,

- Laminar when Re < 2300
- Transitional when 2300 < Re < 4000
- Turbulent when Re > 4000

$$Re = \rho UD/v$$

Where:

- ρ is the density (kg/m^3)
- U is the mean velocity of the flow (m/s)
- D is the hydraulic diameter (m)
- v is the kinematic viscosity (Viscosity is another factor may affect the fluid flow. There are two types of viscosity: dynamic viscosity and kinematic viscosity. Kinematic viscosity is the customarily measured one.)

3.2.2 Navier-Stokes Equation

CFD applies numerical methods to solve the fluid flow governing equations, the Navier-Stoke Equations are known as the conservation law for Newtonian fluids, the equations for mass, momentum and energy conservations (G. Mylavarapu et al., 2009):

$$\frac{\partial \rho}{\partial t} + \frac{\partial}{\partial x_j}\left[\rho u_j\right] = 0$$

$$\frac{\partial}{\partial t}(\rho u_i) + \frac{\partial}{\partial x_j}\left[\rho u_i u_j + p\delta_{ij} - \tau_{ij}\right] = 0, i = 1, 2, 3$$

$$\frac{\partial}{\partial t}(\rho e_0) + \frac{\partial}{\partial x_j}\left[\rho u_j e_0 + u_j p + q_j - u_i \tau_{ij}\right] = 0$$

3.2.3 Governing Equation of Fluid Flow in the Human Upper Airway

There are three main methods to discretize the governing differential equations into algebraic forms, such as Finite Element Method, Finite differencing and Finite Volume Method. The Finite Volume Method (FVM) is based on integral conservation law. In CFD, FVM is used to discretize the governing equations. The advantage of FVM is that it can be utilized in both structured and non-structure mesh.

In this project, all calculations were performed in ANSYS-CFX, which is based on the Finite Volume Method (FVM), which is used to solve the Navier-Stokes equations to achieve the details of fluid flow. The governing equations of fluid flow are reconstructions of the conservation of mass of the fluid and the conservation of momentum. The equations are shown as follows:

Firstly, for a compressible fluid, the mass conservation equation (continuity equation) is presented as:

$$\frac{\partial \rho}{\partial t} + div(\rho u) = 0$$

Secondly, for an incompressible fluid:

$$divu = 0$$

The momentum equations are presented as:

$$\rho \frac{Du}{Dt} = \frac{\partial(-p + \tau_{xx})}{\partial x} + \frac{\partial \tau_{yx}}{\partial y} + \frac{\partial \tau_{zx}}{\partial z} + S_{Mx}$$
$$\rho \frac{Dv}{Dt} = \frac{\partial \tau_{xy}}{\partial x} + \frac{\partial(-p + \tau_{xy})}{\partial y} + \frac{\partial \tau_{zy}}{\partial z} + S_{My}$$
$$\rho \frac{Dw}{Dt} = \frac{\partial \tau_{xz}}{\partial x} + \frac{\partial \tau_{yz}}{\partial y} + \frac{\partial(-p + \tau_{zz})}{\partial z} + S_{Mz}$$

Where:

- ρ is the density (kg/m^3)
- **u** is velocity vector
- p is pressure (Pa)
- τ is stress component

These equations govern fluid flow inside the human airway.

3.3 Meshing and Geometrical Modification

The mesh was set up using the Meshing™ in ANSYS Workbench version 18.2, the adequacy of mesh density is determined by verifying the results based on a steady-state flow rate, and conducted by investigating changes in velocity and pressure at the monitoring point.

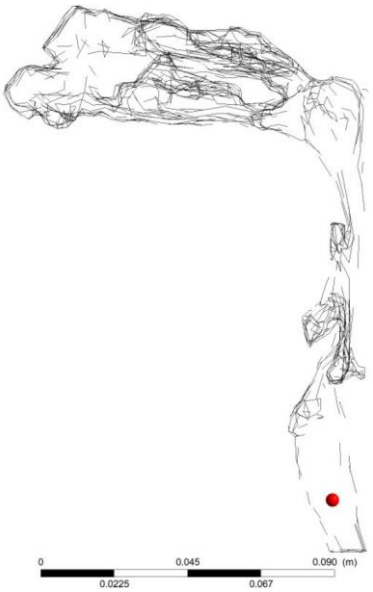

Figure 3.2: Location of the monitoring point.

This project aimed to model and simulate the airflow through the human upper airway. A monitoring point was prescribed in the middle of the larynx to track the changes in pressure and flow behaviours, and this location was chosen because the preliminary work showed that there were very little differences in simulated results as a function of the location of monitoring points in the vicinity of the monitoring point used in the study, the monitoring point provides insights into how flow downstream may be affected by the subtle differences in the location of the epiglottis relative to the back pharyngeal wall.

Mesh independence analysis was performed to ensure that the results were insensitive to the density of mesh. There were four different meshes involved in the mesh independence study. **Table 1** shows the summary of the four different mesh configurations. Mesh independence tests were performed using a constant flow rate of 5.0 L/s (T. Lai, 2011), which is the peak flow rate during respiration. As the Reynolds Number exceeds 2800 at the inlet boundary (the two nostrils), a turbulence model was used for the transient simulation. ANSYS has at least 16 turbulence models, and BSL Reynolds Stress model was used to predict the airflow behaviours within the human upper airway (T. Lai, 2011).

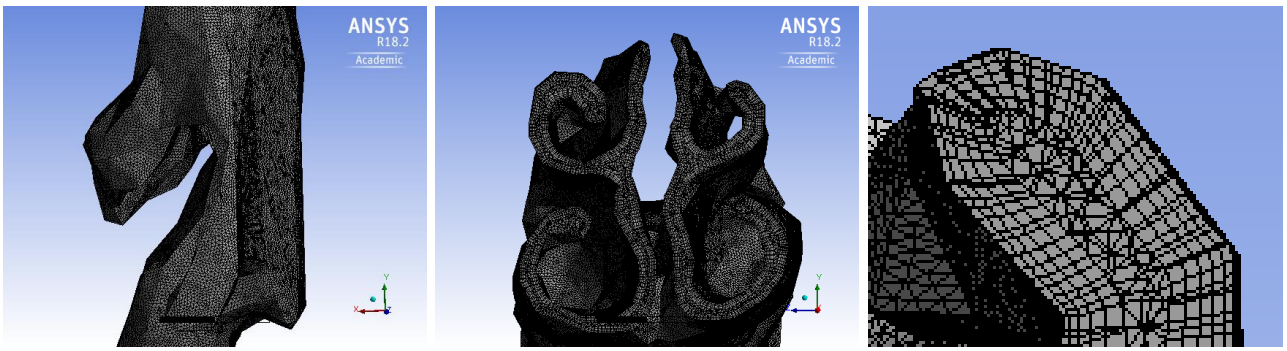

Figure 3.3: Detailed mesh illustration of the computational model. Mesh overall at the epiglottis (a), cross-sectional view of the nasal cavity (b), mesh detail with inflations at the walls (c).

Table 1: Summary and results of the mesh independence study.

Grid	Cells Number	Velocity (m/s)	Difference	Pressure (Pa)	Difference
1	3500k	25.3	0.00%	2670	0.00%
2	5500k	35.4	39.92%	2617	1.98%
3	7500k	38.7	9.32%	2633	0.61%
4	9500k	37.5	2.07%	2630	0.11%

Results of the mesh independence study show that there is an exponential decrease in the change in velocity and pressure as a function of the cell number. When the number of cells exceeds 7500k, there is less than 3% change in velocity and pressure at the monitoring point, which suggests that grid option 3 is a reasonable mesh density used for the simulations.

The distance between epiglottis tip and the back pharyngeal wall is 6.00mm in the original model, and five models have been reconstructed (modified from the original model) by varying the distance between the epiglottis tip and the back pharyngeal wall. The models are defined as Model 1, Model 2, Model 3, Model 4 and Model 5 for discussion purposes with the last model having the least distance between the epiglottis tip and the back pharyngeal wall.

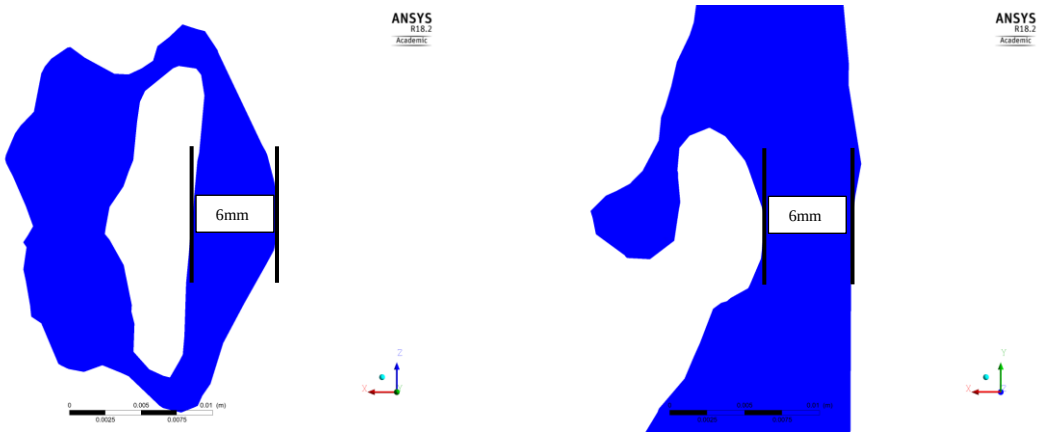

Figure 3.4: Cross-sectional view and mid-sagittal view of the upper airway model at the epiglottis level to show the difference in distances between the epiglottis tip and the back of the pharyngeal wall.

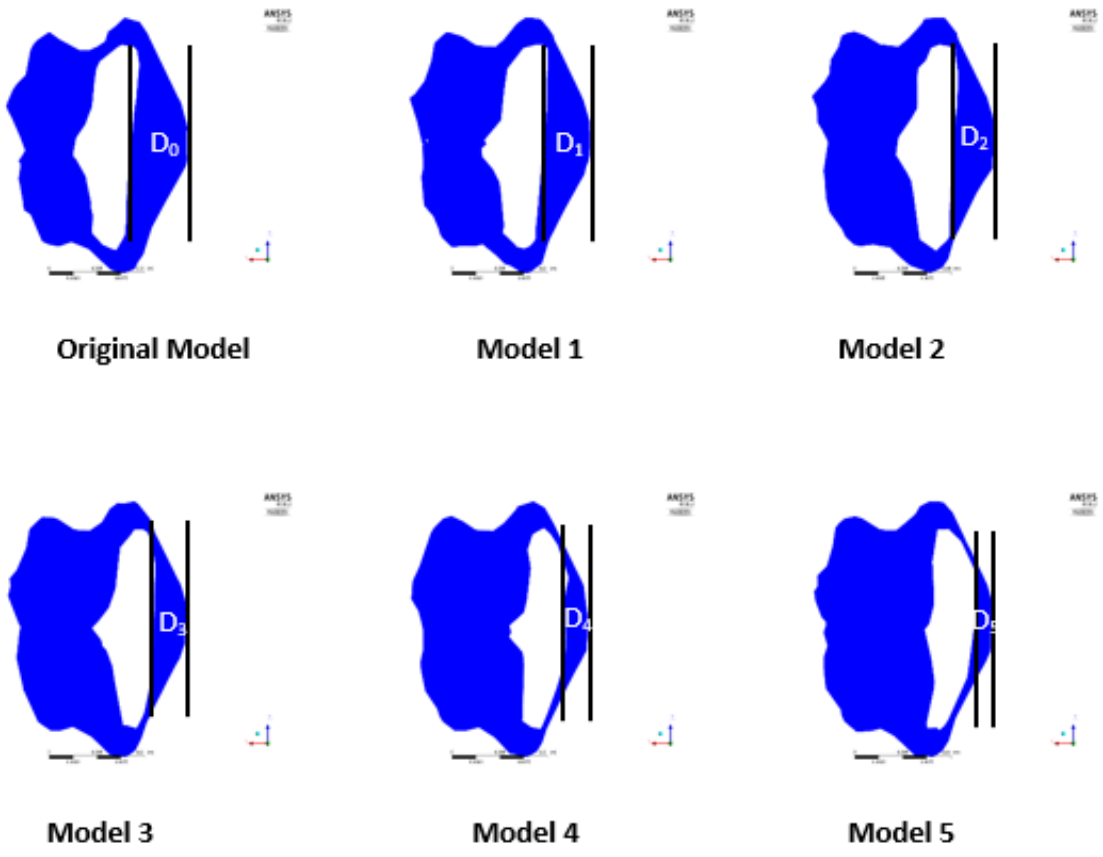

Figure 3.5: The cross-sectional view after the modification in six different models.

Table 2: Distance between epiglottis tip and the back of the pharyngeal wall.

Models	D (mm)
Original	D_0=6.00
Model 1	D_1=5.00
Model 2	D_2=4.00
Model 3	D_3=3.00
Model 4	D_4=2.00
Model 5	D_5=1.00

3.4 Steady-state Simulations

Commercial ANSYS-CFX (v18.2, ANSYS Inc., Canonsburg, USA) was used to solve the airway flow governing equations. The second order finite volume schemes were applied to discretize the flow governing equations. All the physical specifications of the model are presented as follows:

1. State: Steady-state
2. Turbulence model: BSL Reynolds Stress model
3. Material: The fluid considered here was incompressible air at 25℃
4. Normal air density: 1.29 kg/m^3
5. Viscosity：1.846e-10^{-5} kg/ms
6. Time steps per run: 100
6. 1 ATM（atmospheric pressure at inlet boundaries）
7. No-slip boundary conditions were applied to all airway walls
8. Turbulence intensity: 5%
9. Turbulence viscosity ratio: 10
10. Inlet boundary: two nostrils
11. Inflation: maximum five layers at the walls

3.5 Transient Simulations

For transient flow simulations, as the flow varies with time, the input flow was defined using a time step, ∇t =0.625s for a total respiratory cycle of 5s. As the transient flow simulations were run using the same mesh density as the steady-state model and are precede and continued from a steady-state analysis, time independence of the solution is unlikely to affect the results. A sinusoidal waveform to represent the flow profile as shown in **Figure 1.4** was used: $v = 2\sin\left(\frac{2\pi t}{5}\right) L/s$. Other details of the analysis and boundary conditions for the transient state simulation are similar to those applied for the steady state run and are reiterated as follows to provide clarity.

1. Flow type: Transient
2. Turbulence model: BSL Reynolds Stress model
3. Time steps: 0.625s
4. Time steps per run: 8 (One ideal respiratory cycle is 5.000s)
5. 1 ATM（atmospheric pressure at inlet boundaries）.
6. No-slip boundary conditions were applied to all airway walls
7. Turbulence intensity: 5%
8. Turbulence viscosity ratio: 10
9. Inlet boundary: two nostrils
10. Outlet boundary: larynx
11. Inflation: 5 layers at the walls
12. Normal air density: 1.29 kg/m^3

The conservation law of mass and momentum are showing as below:
Continuity equation:

$$\nabla \cdot (\rho \mathrm{U}) = 0$$

Momentum equation:

$$(\mathrm{U} \cdot \nabla)\mathrm{U} = -\frac{1}{\rho}\nabla p + \nabla \cdot [v(\nabla U + (\nabla U)^T)]$$

Where

- ρ is density
- p is pressure
- U is the mean velocity of the flow
- v is kinematic viscosity

CHAPTER 4

RESULTS AND DISCUSSION

4.1 Steady-state Simulation Results

In this section, the simulation results for the airflow velocity and pressure distributions during a steady state inlet airflow rate of 5.0 L/s will be discussed.

4.1.1 Velocity Distribution

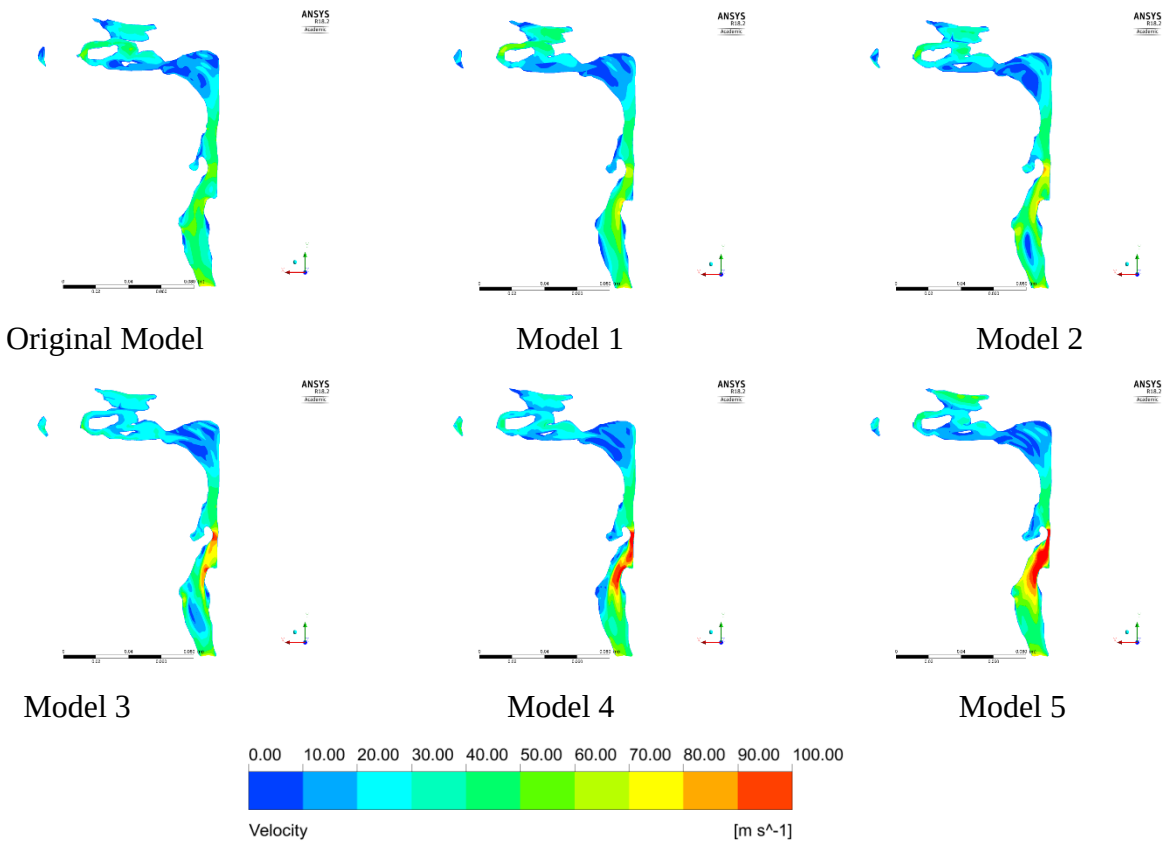

Figure 4.1: Velocity magnitude contours of the models along the middle-sagittal plane under a constant inlet flow rate of 5.0 L/s.

Figure 4.1 shows the contours of the velocity magnitude distribution at the middle-sagittal plane. The maximum velocity is found in the epiglottis region for all the models, and the velocity exceeds 90m/s in models 3, 4 and 5, which may be due to the small cross-sectional area. In addition, results from the figure also demonstrate that the reduction of the airway diameter at the epiglottis appears to change the velocity distribution field more distinctively downstream compared to the top region of the epiglottis. This fact is evident in **Figure 4.2**, which presents the mean values of velocity at the epiglottis level for all the models. The relationship shown in the figure appears to observe a linear trend, and slight discrepancies are likely related to the different node selected in the models due to mesh differences in the six models (including the original).

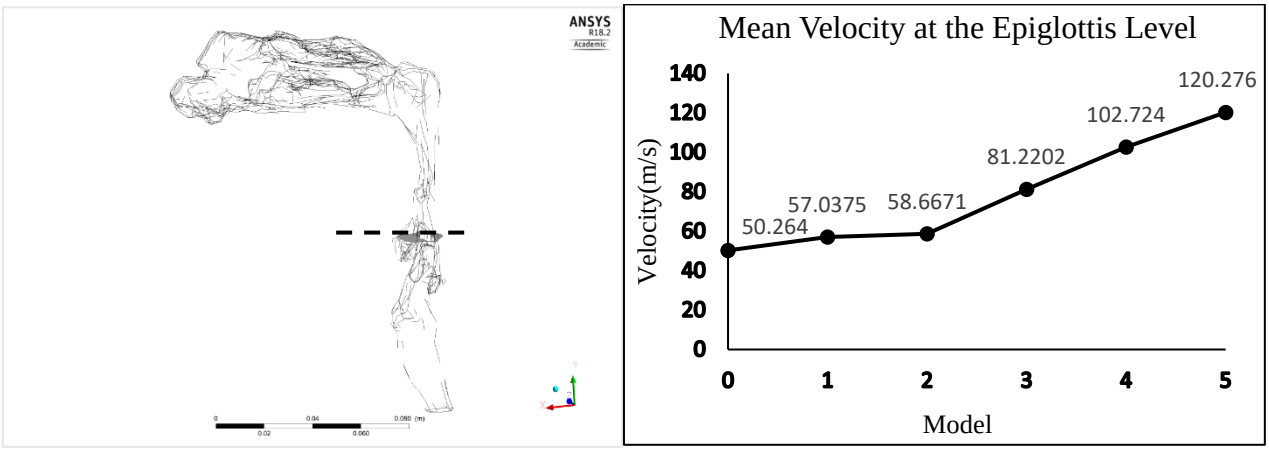

(a) (b)

Figure 4.2: The position of the epiglottis level (a) and the plots of the mean velocity magnitude at this level for all the models (b).

4.1.2 Pressure Distribution

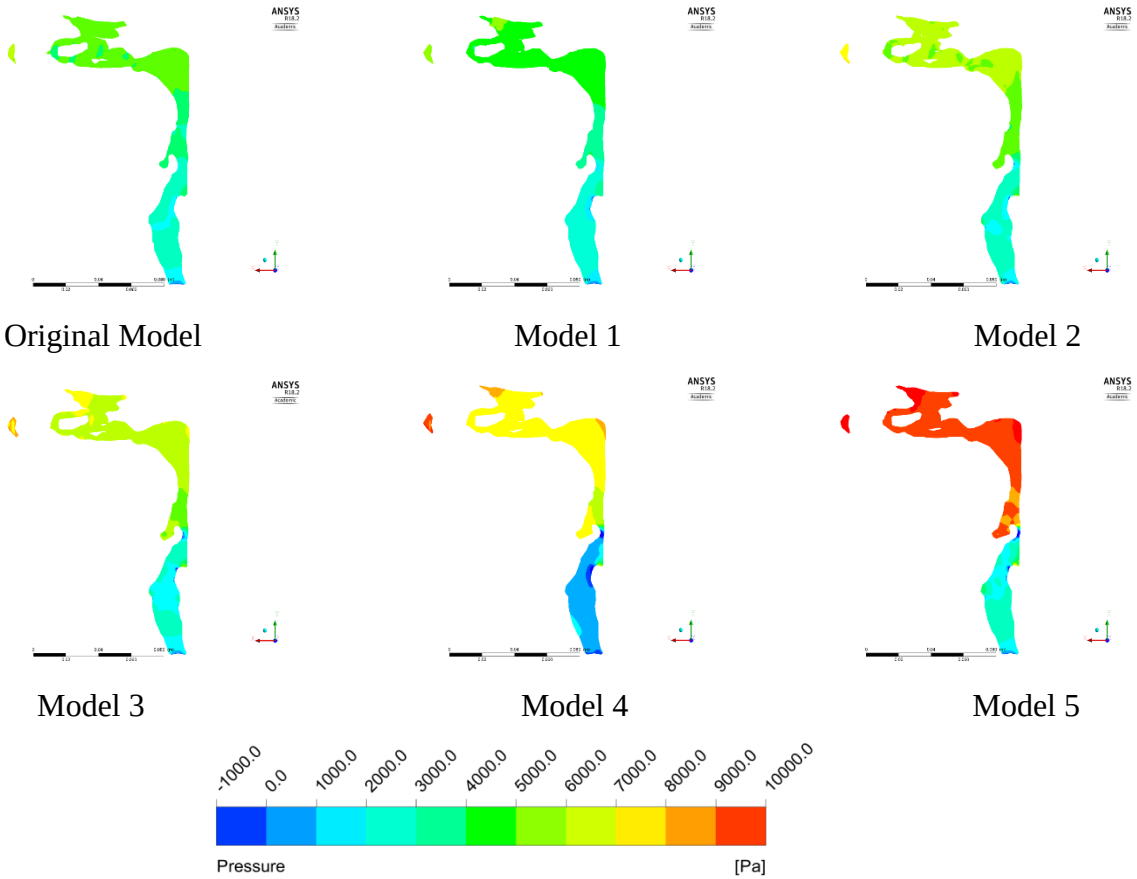

Figure 4.3: Pressure contours of the models along the middle-sagittal plane under a constant inlet flow rate of 5.0 L/s.

Figure 4.3 presents the pressure distribution at the middle-sagittal plane. It is obvious that the pressure magnitude drops from the nasal cavity to the trachea in all the six models with a distinctive pressure drop at the epiglottis level due to the constriction of the airway tract. By decreasing the distance between the epiglottis tip and the back of the pharyngeal wall, the pressure at regions rostral to the epiglottis increases rapidly, from roughly 4000Pa in the Original Model to 10000Pa in Model 5. In addition, in the original Model, Model 1, Model 2 and Model 3, there is no significant difference in pressure at regions caudal to the epiglottis. However, in Model 4, the pressure decrease dramatically in the larynx lumen where the pressure drops from 3000Pa in Model 3 to 1000Pa in Model 4. Interestingly, the pressure increases again to 4000Pa in Model 5. In conclusion, the location of the epiglottis position affects the pressure distribution and further studies to understand the implications of this for various diseases will be of great importance.

4.2 Transient Simulation Results

In this section, the simulation results for the airflow velocity and pressure distributions for a transient inlet airflow rate of $v = 2\sin\left(\frac{2\pi t}{5}\right)\ L/s$ will be discussed. The flow was resolved using a time-step of 0.625s over the duration of the 5.0s respiratory cycle.

4.2.1 Velocity Results

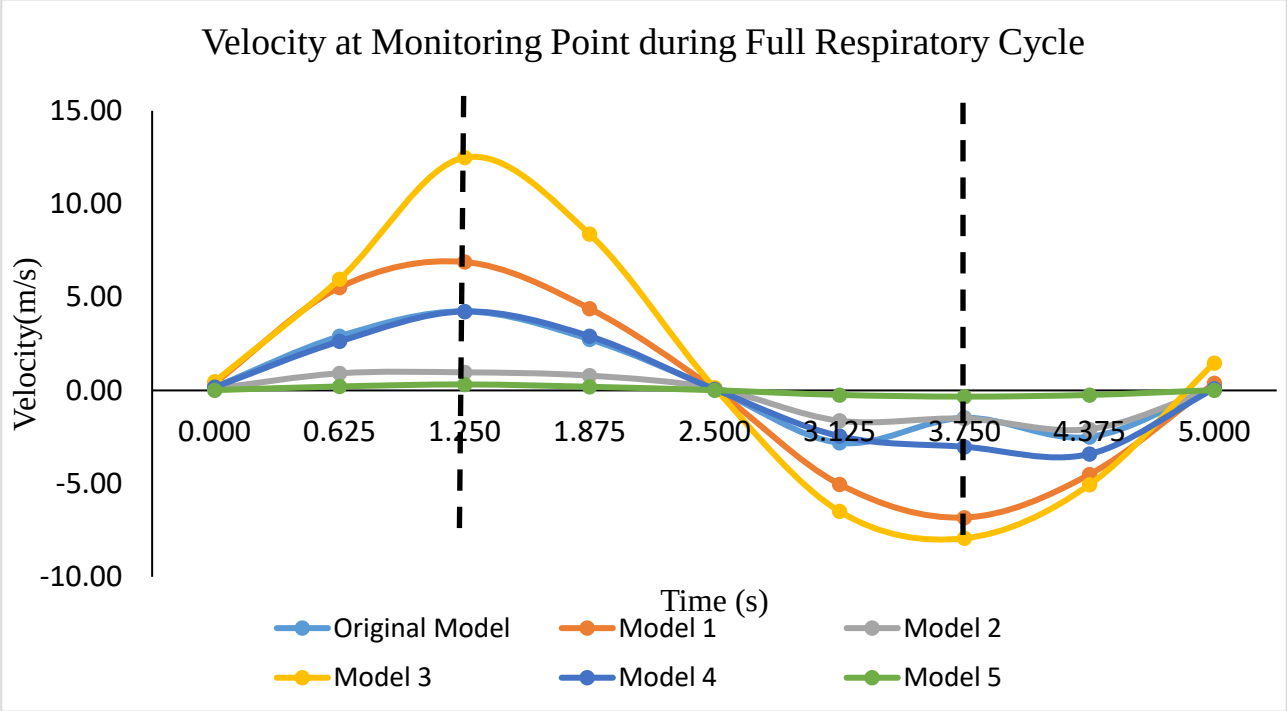

Figure 4.4: Velocity plots at the monitoring point over a full respiratory cycle.

As noted in previous chapters, airflow velocity magnitude and pressure for the full respiratory cycle are investigated in the present research project, and this is a highlight given that majority of existing studies in the literature uses constant flow rate as the inlet flow condition. **Figure 4.4** displays the time history of the velocity at the monitoring point for the different models during a full respiratory cycle. During the inspiratory phase (0 - 2.5s), all the models have similar velocity profiles, and the peak velocity occurs at t = 1.25s. During the expiratory phase, while the Original Model and Model 2 velocity profile has a similar shape, they are different from Models 1, 3, 4 and 5. How the aforementioned observations are related to the structure and position of the epiglottis are unclear and will require further investigations. Last but not least, the time where the peak expiratory flow occurs also appears to have shifted from the original model in Models 1 and 3.

4.2.2 Velocity Distribution

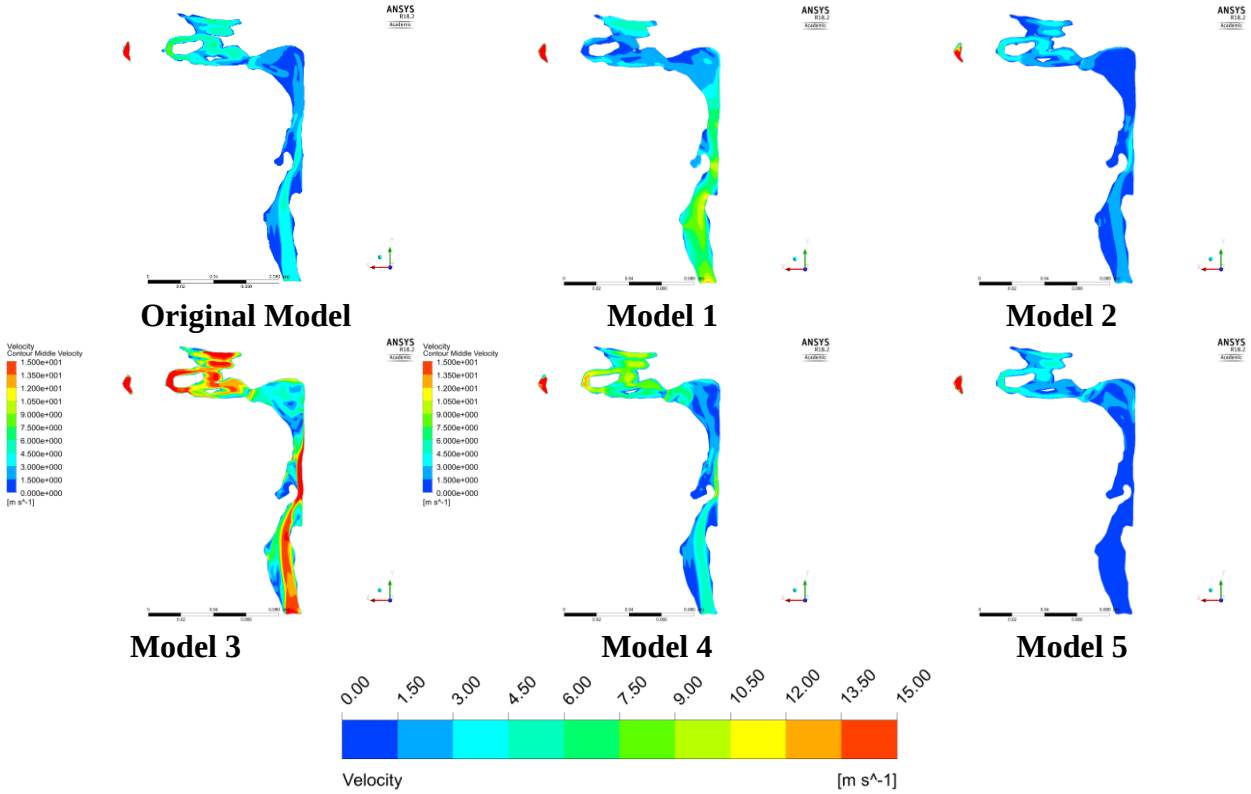

Figure 4.5: Velocity magnitude contours of the models along the middle-sagittal plane at **1.25s**.

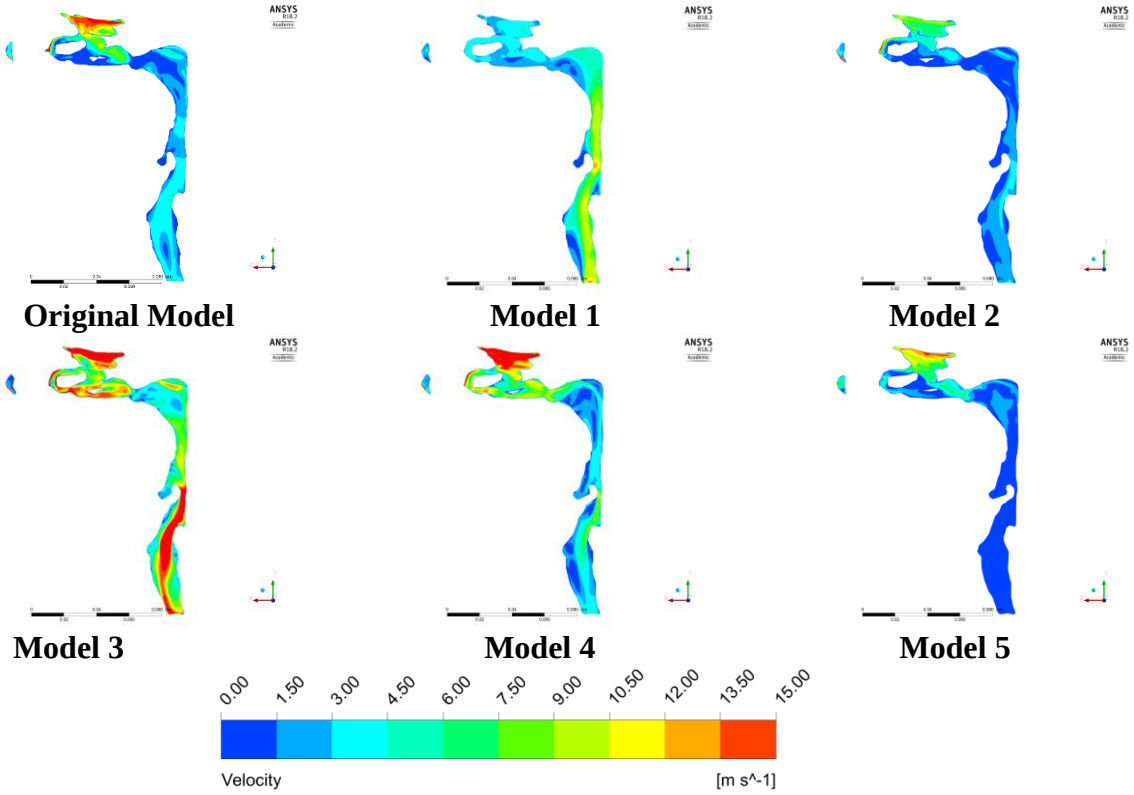

Figure 4.6: Velocity magnitude contours of the models along the middle-sagittal plane at **3.75s**.

Figure 4.5 and **Figure 4.6** demonstrate the velocity magnitude contours at the mid-sagittal plane for the six models at t = 1.25s and 3.75s. The figure shows that there are significant differences in the velocity field distribution pattern between the models at t = 1.25s and 3.75s. By comparing the transient and steady-state solutions, distinctive differences can also be observed, and this is expected since the inlet airflow rate varies with time in the transient simulations, which may have affected the velocity field distribution pattern in the model.

4.2.3 Pressure Distribution

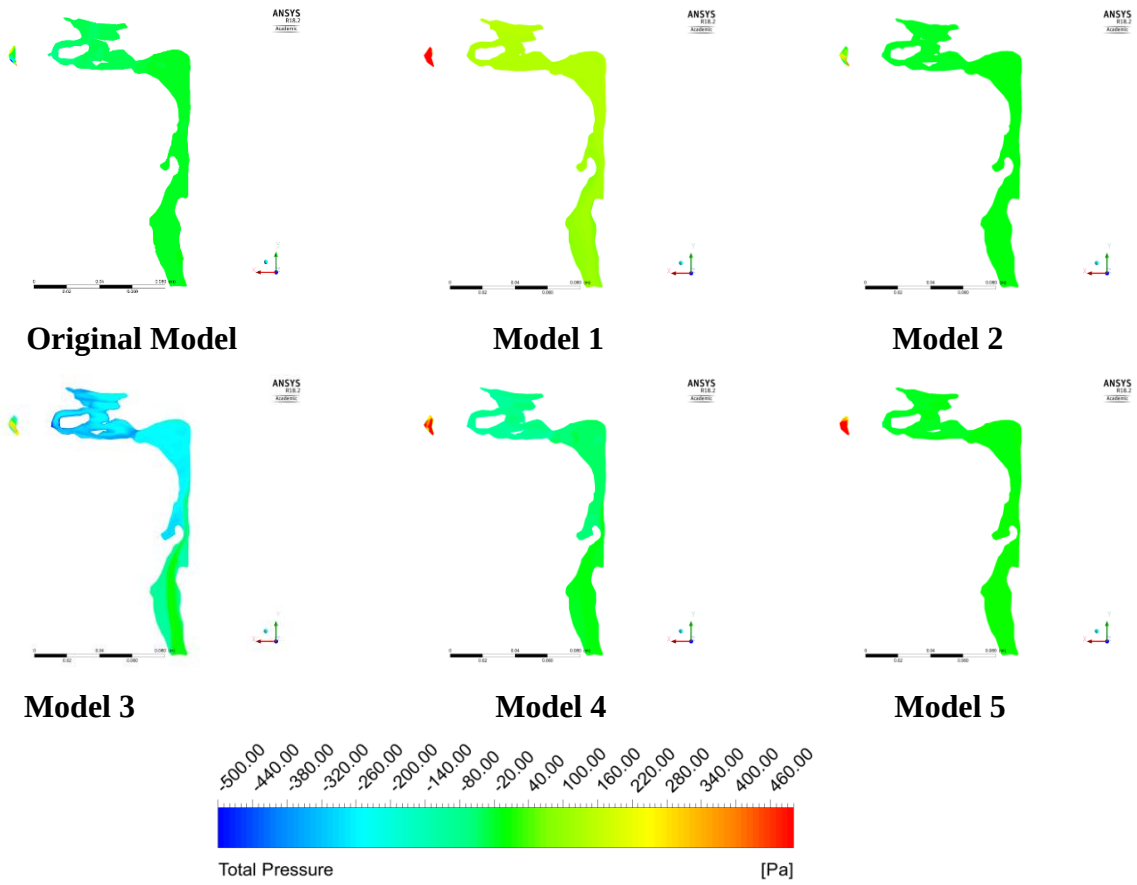

Figure 4.7: Pressure contours (Pa) of the models along the middle-sagittal plane at **1.25s**.

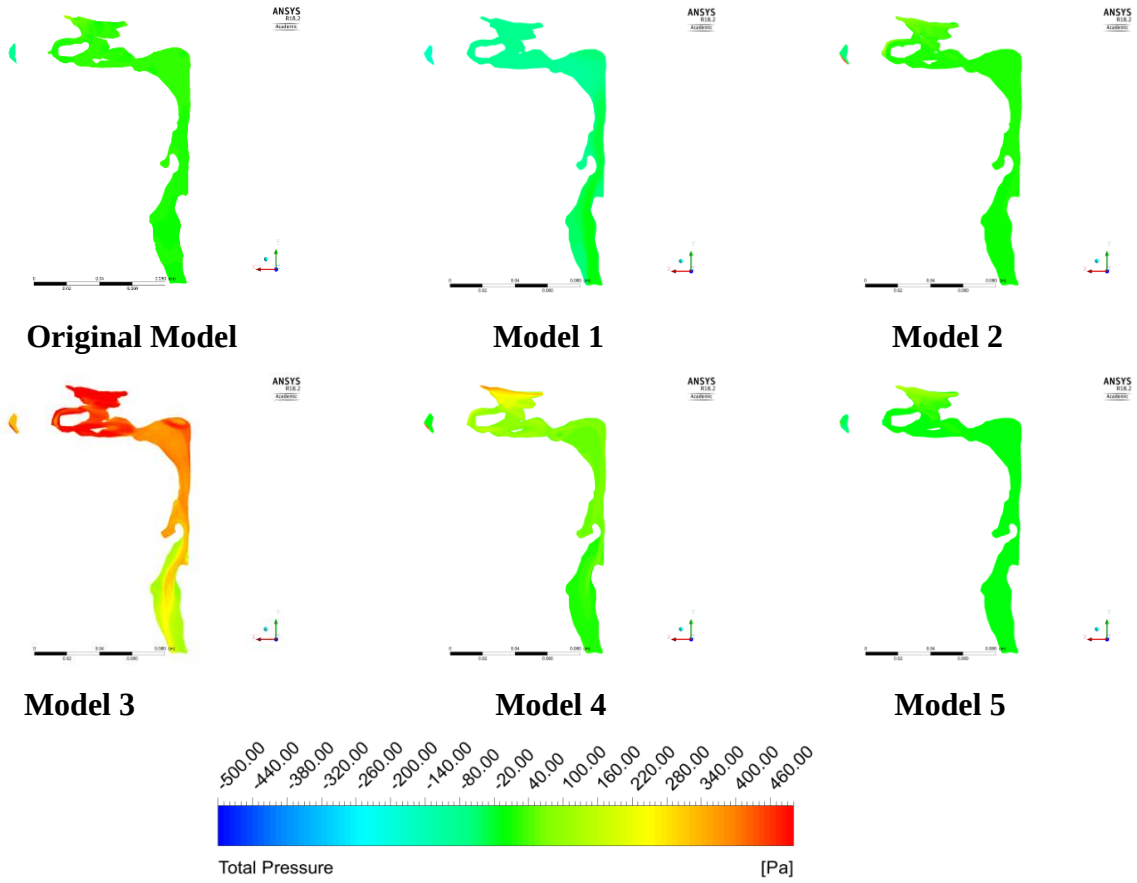

Figure 4.8: Pressure contours (Pa) of the models along the middle-sagittal plane at **3.75s**.

The pressure contours of the models at t = 1.25s and t = 3.75s are presented in **Figure 4.7** and **Figure 4.8** respectively. The pressure magnitude drops from the nasal cavity to the larynx in the Original model at both t = 1.25s and t = 3.75s.

At t = 1.25s, a noticeable change in the overall pressure can be observed in Model 1. In Model 3, the pressure changes significantly in the nasal cavity, and the pressure drops from 50Pa to -350Pa at the nasal cavity. However, similar observations are not made in the other models which suggest that the decreased in airway diameter at the epiglottis level changes pressure upstream of the epiglottis variably.

At t = 3.75s, the main difference between the original model and Model 2 is that the overall pressure drops from 30Pa to -150Pa, with an apparent change in pressure at the nasal cavity. Similar pressure distributions are shown in the Original Model, Model 2 and 5. The pressure in Model 3 appears to increase drastically and exceeds 200Pa in many regions of the airway.

4.2.4 Cross-sectional analysis

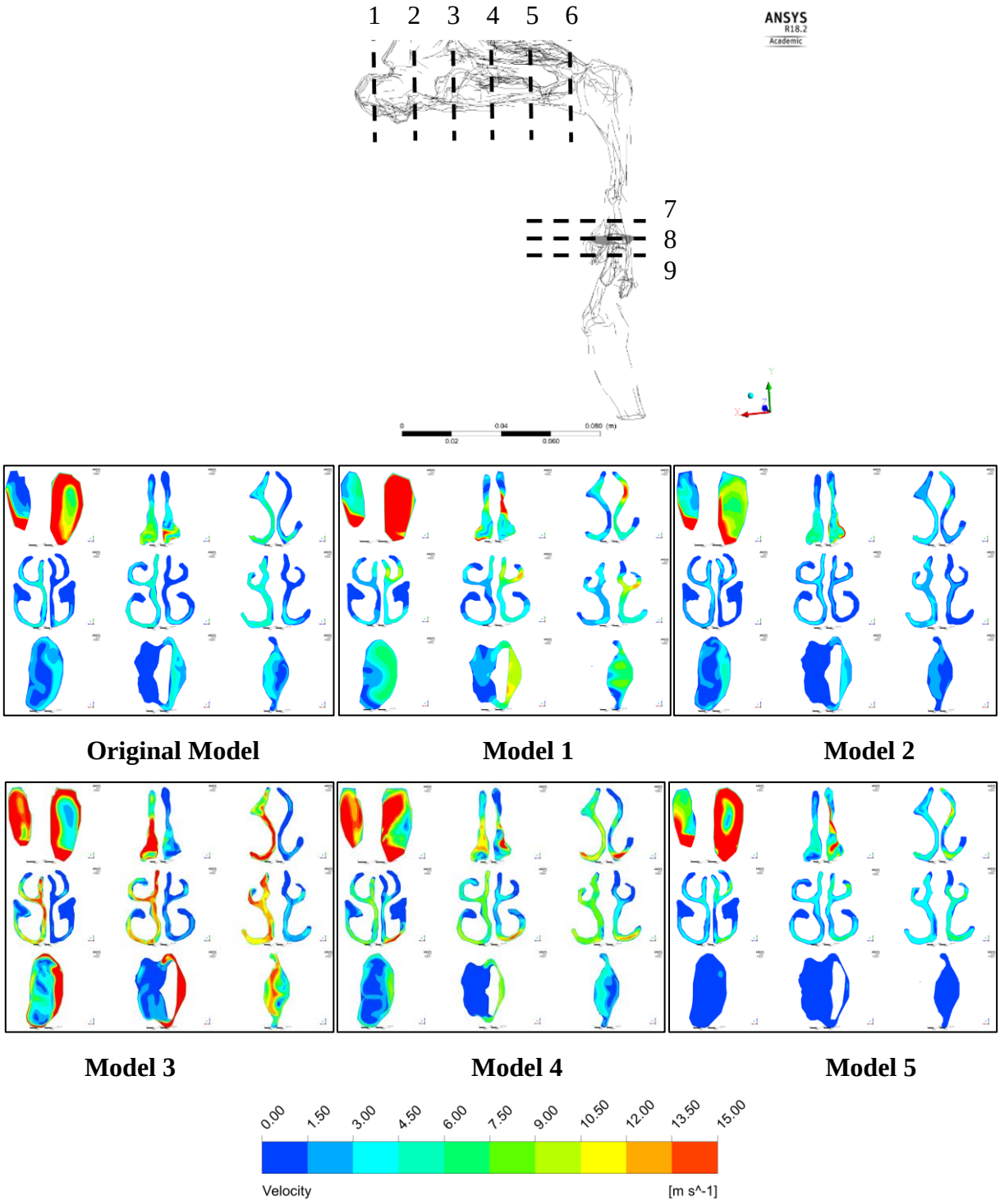

Figure 4.9: Cross-sectional velocity contours at the models at **1.25s**.

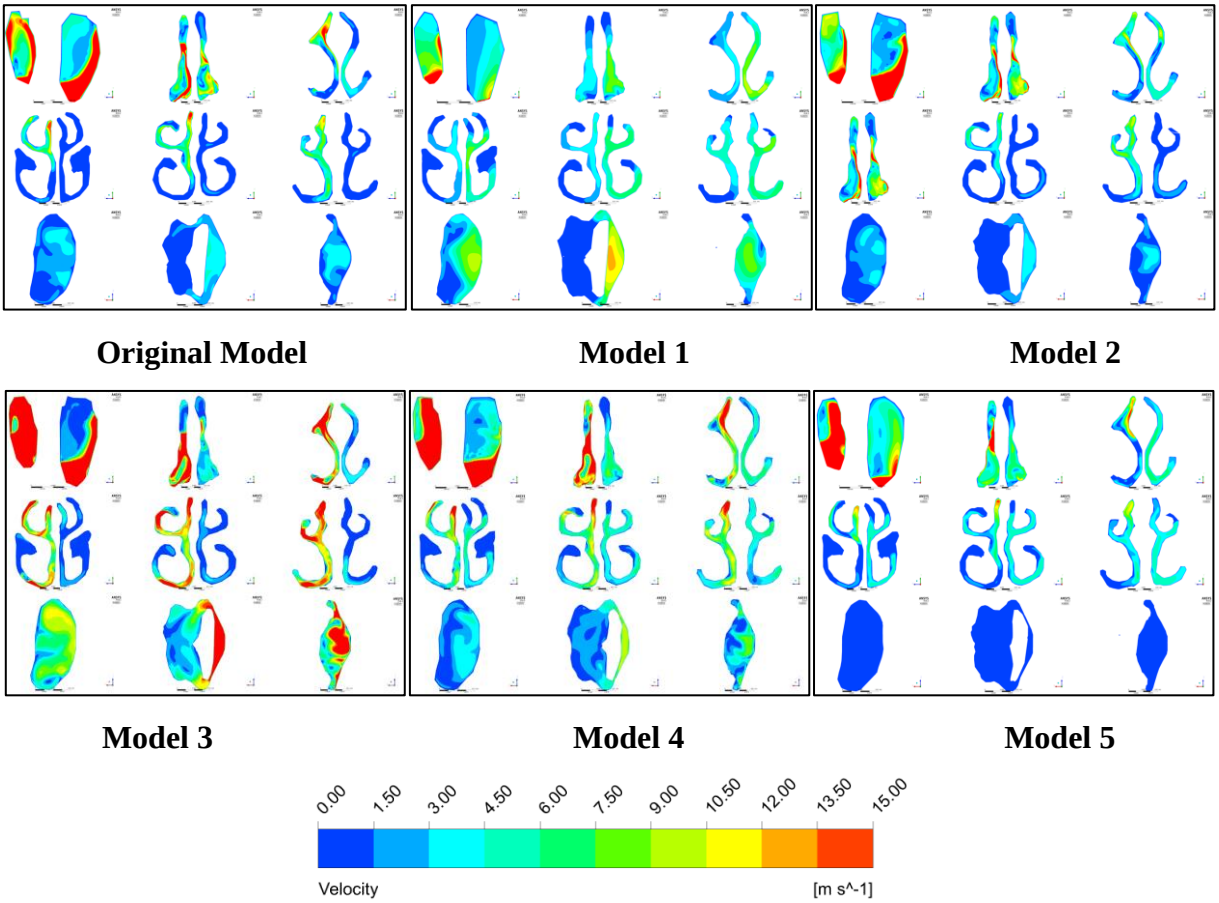

Figure 4.10: Cross-sectional velocity contours at the models at **3.75s**.

To achieve a realistic prediction of airflow in the human upper airway, nine cross-sectional planes have been chosen for analysis, six planes were defined in the nasal cavity, and three planes were defined across the airway at the epiglottis level. **Figures 4.9 and 4.10** show the cross-sectional velocity distribution pattern at t = 1.25s and t = 3.75s. Comparison of the velocity contours in the models with different levels of constriction demonstrates notable differences in the airflow pattern both through the nasal cavity and epiglottis cross-sectional area. Hence, the diameter of the airway at the epiglottis level not only affects the velocity of air passing through the region and the pressure in the airway but also the velocity distribution pattern across the airway cross-sections. For practical reasons and to enable a meaningful discussion, change in flow conditions in the nasal cavity at a specific plane (plane 3) is chosen and discussed as it is on the middle of the nasal passageway. Results from the study show that constriction at the epiglottis affects the location of the maximum velocity such that it shifts between the left and right nasal passageway. Consistent with the results presented in **Figure 4.9** and **4.10**, overall velocity appears to be the highest in model 3 at both t = 1.25s and t = 3.75s. It can also be readily observed that maximum velocity in the nasal cavity of model 3 matches with the velocity behind the epiglottis. The reason for the sharp increase in velocity and pressure from model 2 to model 3 and why it decreases with further constriction of the upper airway diameter behind

the epiglottis is unclear but may suggest the importance of an airway diameter threshold range such that it will affect flow in the upper airway drastically when it is exceeded.

4.3 Summary

In this chapter, CFD simulations were applied to investigate the airflow pattern in six upper airway models under both steady-state and transient flow rates. The velocity and pressure profiles for various diameter at the epiglottis level were presented and discussed. The simulation results show that the position and structure of epiglottis is an important factor that can change the velocity and pressure in the human upper airway variably.

CHAPTER 5

CONCLUSION

5.1 Conclusion

In conclusion, CFD simulations of airflow in the human upper airway were performed to study the effects of epiglottis positions and structures on flow characteristics. Six realistic models were successfully created and simulated using CFD. Also, mesh independence studies were conducted to ensure that accurate results can be obtained, and transient simulation was preceded by a constant flow rate steady state analysis. In the results and discussion section, the velocity and pressure field distributions were presented and discussed, along with velocity distribution pattern at the airway cross-sections.

This research study suggests that the position and structure of epiglottis may be a dominant factor in influencing airflow pattern in the human upper airway and distance between the epiglottis tip and the back of the pharyngeal wall could potentially affect the airflow characteristics. Results also suggest that structure of the airway has influenced over the flow characteristic and velocity distribution pattern at the nasal cavity. While results from the steady-state study are highly coherent with existing work in the literature and demonstrate a systematic and progressive change in velocity and pressure with the change in airway dimensions at the epiglottis level, such changes are a lot more variable in the transient models. The reasons for this is unclear and is currently under investigations, but it is likely related to the choice of large time-steps used in the study. Although the general pressure in the steady state models is higher than some of those presented in the literature (e.g., **Figure 2.7**), it is important to note that the inlet flow used in this study is many folds higher, but still within the physiological limits and hence is realistic. In the transient models, the velocity magnitude monitored at a location caudal to the epiglottis showed variable differences in velocity as a function of the distance between the epiglottis tip and back pharyngeal wall. In addition, the pattern of the velocity distribution profile is also changed distinctively albeit variably with the decrease in upper airway diameter, and this may provide some insights into how distribution of fine particles may be affected. Interestingly, airway diameter at the epiglottis also appears to have the effect of changing the timing of flow reversal at the nasal cavity in the transient models. The findings from both the steady-state and transient simulations suggest that it is important to consider the specific differences in upper

airway anatomical features as this has wide implications from optimizing lung deposition for inhaler-based medicine to the detailed study of mechanisms that underpins the development and treatment of respiratory diseases such as sleep apnea.

5.2 Limitation

There are several limitations in this project that need to be considered when interpreting the data produced from the simulations.

Firstly, the project is entirely based on computational fluid dynamics, and there is no experimental data yet to verify the results. However, the results produced by the model presented in this research matches (in the same order of magnitude) with existing published studies with similar inlet flow and boundary conditions (T. Lai, 2011). Also, given the time frame that has been defined for this work (8 months including literature review), experimental data to validate the results is not feasible but an experiment to provide validation for the simulation presented in this study is currently in progress.

Secondly, although 3D Slicer is capable of producing geometries with high accuracies, the positions of the epiglottis and their structures were modified manually and it has been suspected that this may cause small regional changes in the airway geometry and structure that is adjacent to the epiglottis. Such differences albeit small may cause significant differences in the results given the small diameter of the airway at the epiglottal region. However, further analysis on the airway geometries by comparing the cross-sections of the airway between the models (with different distance between the epiglottis tip and back pharyngeal wall) show that such differences are not presented.

Thirdly, even though the distance between the epiglottis tip and back pharyngeal wall has been accurately defined, there are subtle differences in the structure of the epiglottis among models such that it is slightly bigger in some models. The effect of this on air flow characteristics is unclear since they do not form a critical component along the pathway of the airway lumen and further studies would be required to determine this.

Another limitation is that the flow rate chosen in this study was very high for inhalation simulation with the objective to study the extreme cases of deep inhalation which is relevant when using dry powder inhalers. Also, it is important to note that the velocity, though high is common during

moderate exercise condition (T. Lai, 2011). Further study to understand how lower rate affects the flow field in the upper airway flow is currently underway

Finally, due to time limitations, a course time-step has been used to simulate the models, and detailed discussion on the change in both velocity and pressure is hence not possible here, and this will be refined in future studies. In addition, existing ongoing work to validate the accuracy of the models using other turbulence numerical scheme are also in progress. For example, LES (Large Eddy Simulation) is currently used to re-simulate the models, and it is expected that this will shed light on the variable change in velocity and pressure as a function of the distance between the epiglottis top and back pharyngeal wall.

5.3 Future Work

This project has been undertaken within a limited time frame of approximately eight months including the literature review and works to refine the model and repeated studies and analysis to resolve some of the limitations explained above are currently ongoing. This project forms part of a more significant project for a Ph.D. program where the objective is to understand airflow in patient-specific airways and the implications in particle transport and deposition. Firstly, this project only investigated airflow within the human upper airway and hence a comprehensive understanding of particle deposition in the lungs will require the inclusion of the lower respiratory airway, which will be an improvement that will be incorporated in the presented model. Secondly, although this study forms the basis of understanding particle deposition in the airways, particle simulation has not been investigated, but this is currently in progress in a separate project. Finally, as mentioned, experimental data to validate the simulations is important, and the experiment is currently undertaken through the development of a particle imaging velocimetry system.

References

Cheng, S., Brown, E. C., Hatt, A., Butler, J. E., Gandevia, S. C., Bilston, L. E.(2014) Healthy humans with a narrow upper airway maintain patency during quiet breathing by dilating the airway during inspiration. *Journal of Physiology*. 592, 21, 4763-4774.

Cheng, S., Butler, J. E., Gandevia, S. C., Bilston, L. E. (2011) Movement of the human upper airway during inspiration with and without inspiratory resistive loading. *Journal of Applied Physiology*. 110, 1, 69-75.

Cheng, S., Butler, J. E., Gandevia, S. C. & Bilston, L. E. (2008) Movement of the tongue during normal breathing in awake healthy humans. *Journal of Physiology*. 586, 17, 4283-4294.

Cheng, S., David F., Sarah H., Marcus S., Lynne B. (2014) Effect of fluid structure interaction in a three dimensional model of the spinal subarachnoid space. *Journal of Biomechanics*. 47(2014) 2826-2830.

Zhao M, Barber T., Cistulli P., Sutherland K., Rosengarten G. (2013) Computational fluid dynamics for the assessment of upper airway response to oral appliance treatment in obstructive sleep apnea. *Journal of Biomechanics* 46 (2013) 142-150.

Li C., Jiang J., Dong H., Zhao K. (2017) Computational modeling and validation of human nasal airflow under various breathing conditions. *Journal of Biomechanics.*

Bates A. J., Schuh A., Amine-Eddine G., McConnell K., Loew W., Robert J, Flech, Jason C. W., Charles L. D., Raouf S. A. (2017) Assessing the relationship between movement and airflow in the upper airway using computational fluid dynamics with motion determined from magnetic resonance imaging. *Clinical Biomechanics.*

Goutham M., Shanmugam M., Mihai M., Maninder K., Sid K., Ephraim G. (2009) Validation of computational fluid dynamics methodology used for human upper airway flow simulations. *Journal of Biomechanics, 42(2009),* 1553-1559.

Phuong N. L., Ito K. Investigation of flow pattern in upper human airway including oral and nasal inhalation by PIV and CFD. *Building and Environment* 94 (2015) 504-515.

Elin A, Sverre G. Johnsen, Are J. Simonsen, Bernhard Muller. (2017) CFD simulations of turbulence flow in the human upper airways. *Journal of Biomechanical Engineering 12th international Conference on CFD in Oil and Gas, Metallurgical and Process Industries.*

Wei W., Huang S., Chen L., Qi Y., Qiu Y., Li S.. Air flow behavior changes in upper airway caused by different head and neck positions: Comparison by computational fluid dynamics. *Journal of Biomechanics* 52(2017) 89-94.

Yu C., Hsiao H., Tseng T., Lee L., Yao C., Chen N., Wang C., Chen Y. (2012) Computational Fluid Dynamics Study of the Inspiratory Upper Airway and Clinical Severity of Obstructive Sleep Apnea. *The Journal of Craniofacial Surgery* 23(2012) 401-405.

Rahiminejad M., Haghighi A., Dastan A., Abouali O., Farid M., Ahmadi G., (2016) Computer simulations of pressure and velocity fields in a human upper airway during sneezing. *Computers in Biology and Medicine* 71(2016) 115-127.

Nie P., Xu X., Tang Y., Wang X., Xue X., Wu Y., Zhu M., (2015) Computational Fluid Dynamics Simulation of the upper airway of Obstructive Sleep Apnea Syndrome by Muller Maneuver. *Huazhong Univ Sci Technolomputers* 35(3): 464-468, 2015.

Tan J., Huang J., Yang J., Wang D., Liu J., Liu J. Lin S., Li C. Lai H., Zhu H. Hu X., Chen D., Zheng L., (2013) Numerical simulation for the upper airway flow characteristics of Chinese patients with OSAHS using CFD models. *Eur Arch Otorhinolaryngol* 270:1035–1043.

Mihaescu M. Murugappan S., Gutmark E, Donnelly L. F., Khosla S., Kalra M., 2008. Computational Fluid Dynamics Analysis of Upper Airway Reconstructed From Magnetic Resonance Imaging Data. *Annals of Otology, Rhinololy & Laryngology 117(4):303-309.*

Arens, R., McDonough, J.M., Corbin, A.M., Rubin, N.K., Carroll, M.E., Pack, A.I., Liu, J., Udupa, J.K., 2003. Upper airway size analysis by magnetic resonance imaging of children with obstructive sleep apnea syndrome. *American Journal of Respiratory and Critical Care Medicine 167 (1)*, 65–70.

Yu C., Hsiao H., Tseng T., Lee L., Yao C, Chen N, Wang C, Chen Y. (2012) Computational fluid dynamics study of the inspiratory upper airway and clinical severity of obstructive sleep apnea. *The Journal of Craniofacial Surgery* 23:401-405.

Goodarzi-Ardakani V., Taeibi-Rahni M., Salimi M.R., Ahmadi G. (2016) Computational simulation of temperature and velocity distribution inhuman upper respiratory airway during inhalation of hot air, *Respiratory Physiology & Neurobiology* 223(2016) 49-58.

Fan Y., Cheung L, Chong M, Chua H, Chow K., and Liu C. (2011) Computational Fluid Dynamics Analysis on the Upper Airways of Obstructive Sleep Apnea Using Patient – Specific Models. *IAENG International Journal of Computer Science* 38:4.

Aittokallio T., Gyllenberg M., Polo O. (2001). A model of a snorer's upper airway. *Mathematical Biosciences* 170(2001) 79-90.

Fedorov A., Beichel R., Kalpathy-Cramer J., Finet J., Fillion-Robin J. C., Pujol S., Bauer C., Jennings D., Fennessy F., Sonka M, Buatti J., Aylward S, Miller J. V., Pieper S., Kikinis R.. 3D Slicer as an image computing platform for the Quantitative. *Magnetic Resonance Imaging* 30 (2012) 1323–1341.

Jeong S. J., Kim W. S., Sung S. J. Numerical Investigation on the flow characteristics and aerodynamic force of the upper airway of patient with obstructive sleep apnea using computational fluid dynamics. *Medical Engineering & Physics* 29(2007) 637-651.

Lucey A. D., King A. J. C., Tetlow G. A., Wang J., Armstrong J. J., Leigh M. S., Paduch A., Walsh J. H., Sampson D. D., Eastwood P. R. Hillman D. R.. Measurement, Reconstruction, and Flow-Field Computation of the Human Pharynx with Application to Sleep Apnea. *IEEE Transactions on Biomedical Engineering* VOL., 57, No. 10, Oct. 2010.

Xu C., S. Sin H., McDonough J. M., Udupa J. K., Guez A., Arens R., Wootton D. M. Computational fluid dynamics modeling of the upper airway of children with obstructive sleep apnea syndrome in steady flow. *Journal of Biomechanics* 39 (2016) 2043-2054.

Collins T. P., Tabor G. R., Young P. G. A computational fluid dynamics study of inspiratory flow in orotracheal geometries. *Medical and Biological Engineering* (2007) 45:829-836.

Martonen T. B., Quan L., Zhang Z., C. Musante J. Flow Simulation in the Human Upper Respiratory Tract. Cell Biochemistry and Biophysics Vol. 37, 2002.

Gokcan M. K., Gunaydinoglu E., Durtulus D. F. Effect of glottis geometry on breathing: three-dimensional unsteady numerical simulation of respiration in a case with congenital glottis web. Eur. *Arch. Orhinolaryngol* (2016) 273:3219-3229.

Lai T. The degree of doctor of philosophy thesis of Computational fluid dynamic modelling of particle deposition in human upper airways (2011).

Goutham M. The degree of doctor of philosophy thesis of Computational flow modelling of human upper airway breathing. (2013)